Extracting anisotropic μ-type spectral distortions

Mathieu Remazeilles

The University of Manchester

Remazeilles & Chluba
arXiv:1802.10101

"Probing fundamental physics with CMB spectral distortions"
CERN TH Institute, 12-16 Mar 2018

μ-type CMB spectral distortions

Sunyaev & Zeldovich 1970

- At redshifts $10^4 < z < 2\times10^6$ (pre-recombination), energy injections into primordial plasma prevent brehmsstrahlung and double Compton scattering to create photons to maintain Planck's equilibrium, leading to Bose-Einstein equilibrium:

$$n_{BE} \approx n_{Pl} + \mu \frac{e^x}{(e^x - 1)^2}\left(\frac{x}{2.19} - 1\right)$$

$x \equiv h\,\nu / k\,T_{CMB}$

CMB blackbody spectrum

spectral signature of μ-distortion

- Caused by exciting physics processes occurring at redshifts $z > 10^4$:
  - → *dissipation of small-scale acoustic modes* – *Silk 1968*
  - → *annihilation/decay of relic particles* – *Hu & Silk 1993*
  - → *evaporation of primordial black holes* – *Carr et al 2010*

- LCDM predicts: $|\mu| = 2.3 \times 10^{-8}$ → very faint signal! – *Chluba 2016*

  COBE/FIRAS constraint: $|\mu| < 9 \times 10^{-5}$ – *Fixsen et al 1996*

Anisotropic μ-type distortions

Pajer & Zaldarriaga 2012
Ganc & Komatsu 2012
Chluba et al 2017
Ravenni et al 2017

Aside from CMB monopole distortions...

Primordial non-Gaussianity in the ultra-squeezed limit predicts:

- **Anisotropies of μ-type distortions** (*spectral-spatial distortions*):

$$C_\ell^{\mu\times\mu} = 144\, C_\ell^{TT,\mathrm{SW}}\, f_{\mathrm{NL}}^2\, \langle\mu\rangle^2$$

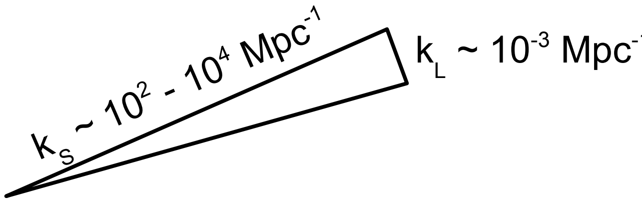

- **μ-T correlations** between CMB temperature and μ-distortion anisotropies:

$$C_\ell^{\mu\times T} = 12\, C_\ell^{TT,\mathrm{SW}}\, \rho(\ell)\, f_{\mathrm{NL}}\, \langle\mu\rangle$$

- **Scale-dependent** $f_{NL}(k) = f_{NL}(k_0)(k/k_0)^{n_{NL}-1}$ with running index of $n_{NL} \le 1.6$ would allow for:

  $f_{NL}(k_0 = 0.05\ \mathrm{Mpc}^{-1}) \approx 5$ ← CMB temperature anisotropies

  $f_{NL}(k = 740\ \mathrm{Mpc}^{-1}) \approx 4500$ ← μ-type distortion anisotropies

Questions

- *Can we detect the μ-T correlated signal with future CMB satellites?*

- *What limit on $f_{NL}(k=740\ \mathrm{Mpc}^{-1})$ can be achieved in the presence of foregrounds?*

Spectral signature of distortions

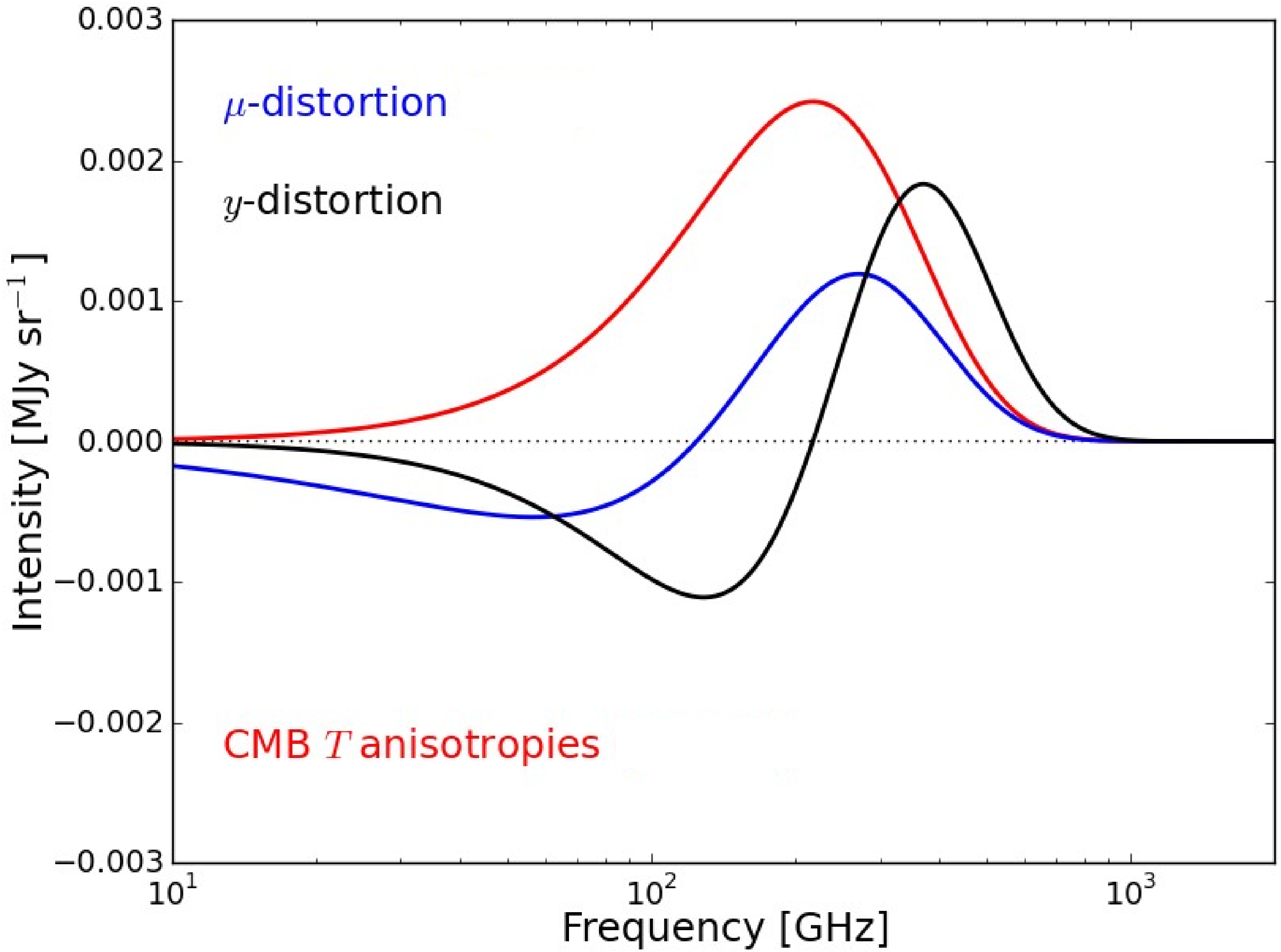

Distinct spectral signatures!
→ Multi-frequency observations allow (in principle) to disentangle those signals

CMB satellite concepts

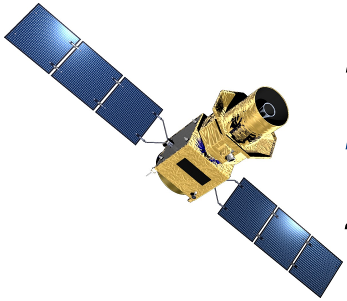

LiteBIRD (JAXA)

Matsumura et al, 2013

40 – 402 GHz ; 2.5 μK.arcmin

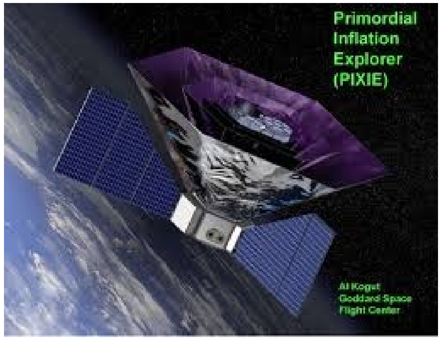

PIXIE (NASA?)

Kogut et al., 2011

30 – 6000 GHz ;

6.6 μK.arcmin *(Δν=30 GHz)*

CORE (ESA? ISRO?)

Delabrouille et al, 2017

60 – 600 GHz ; 1.7 μK.arcmin

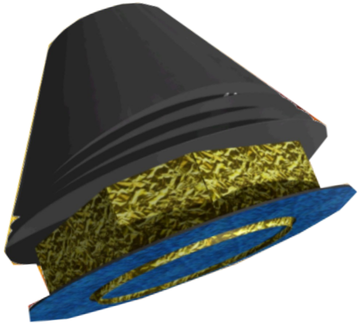

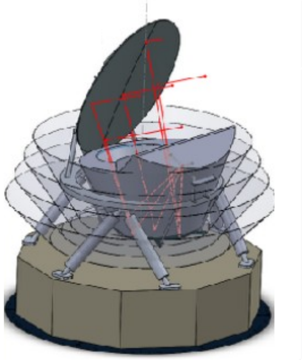

PICO (NASA?)

S. Hannany, priv. comm.

21 – 800 GHz ; 1.1 μK.arcmin

Anisotropic primordial spectral distortions

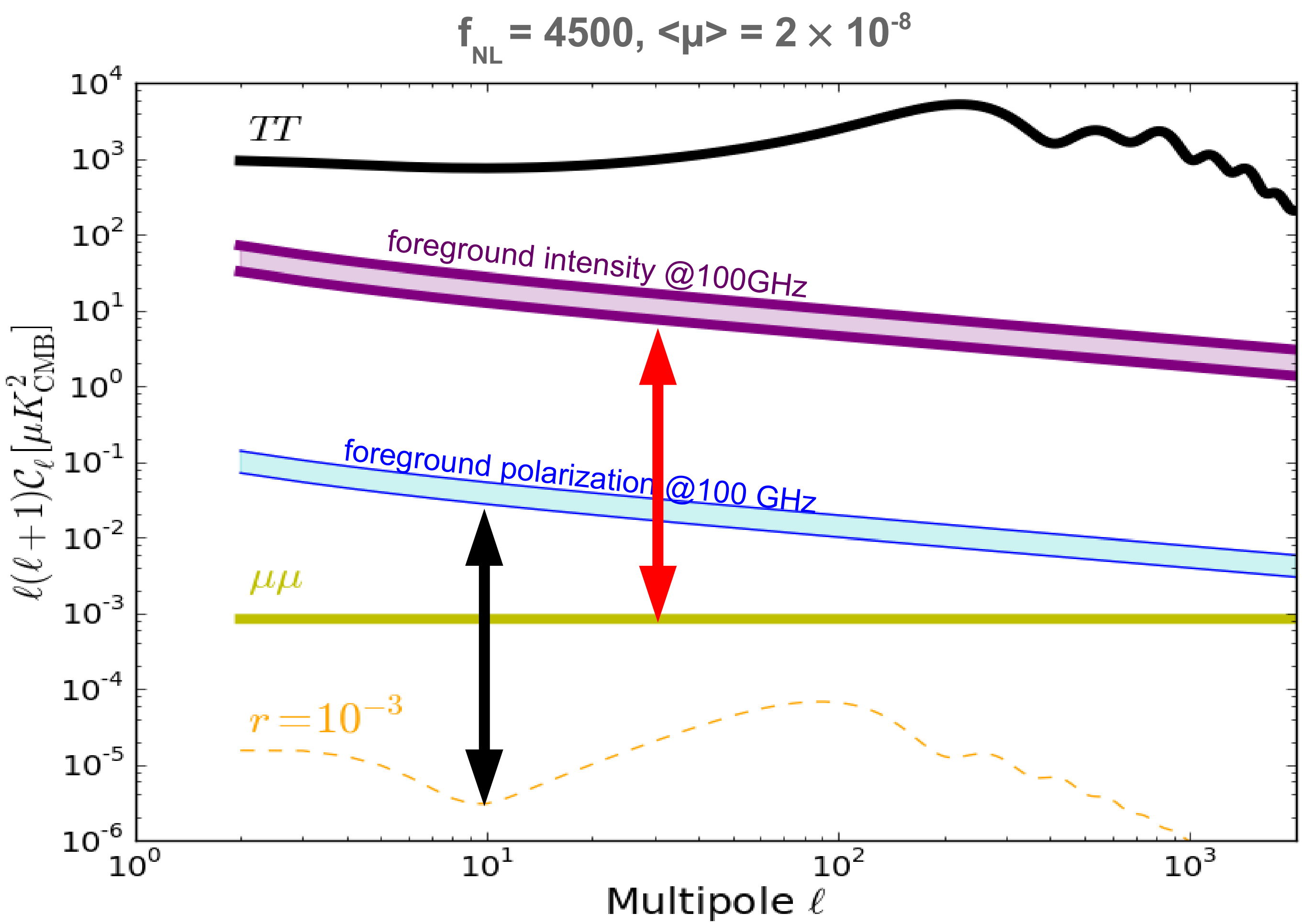

Similar dynamic range between signal and foregrounds than primordial B-modes at r ~ 10^{-3}

→ to be definitely considered by future CMB satellites...

Anisotropic primordial spectral distortions

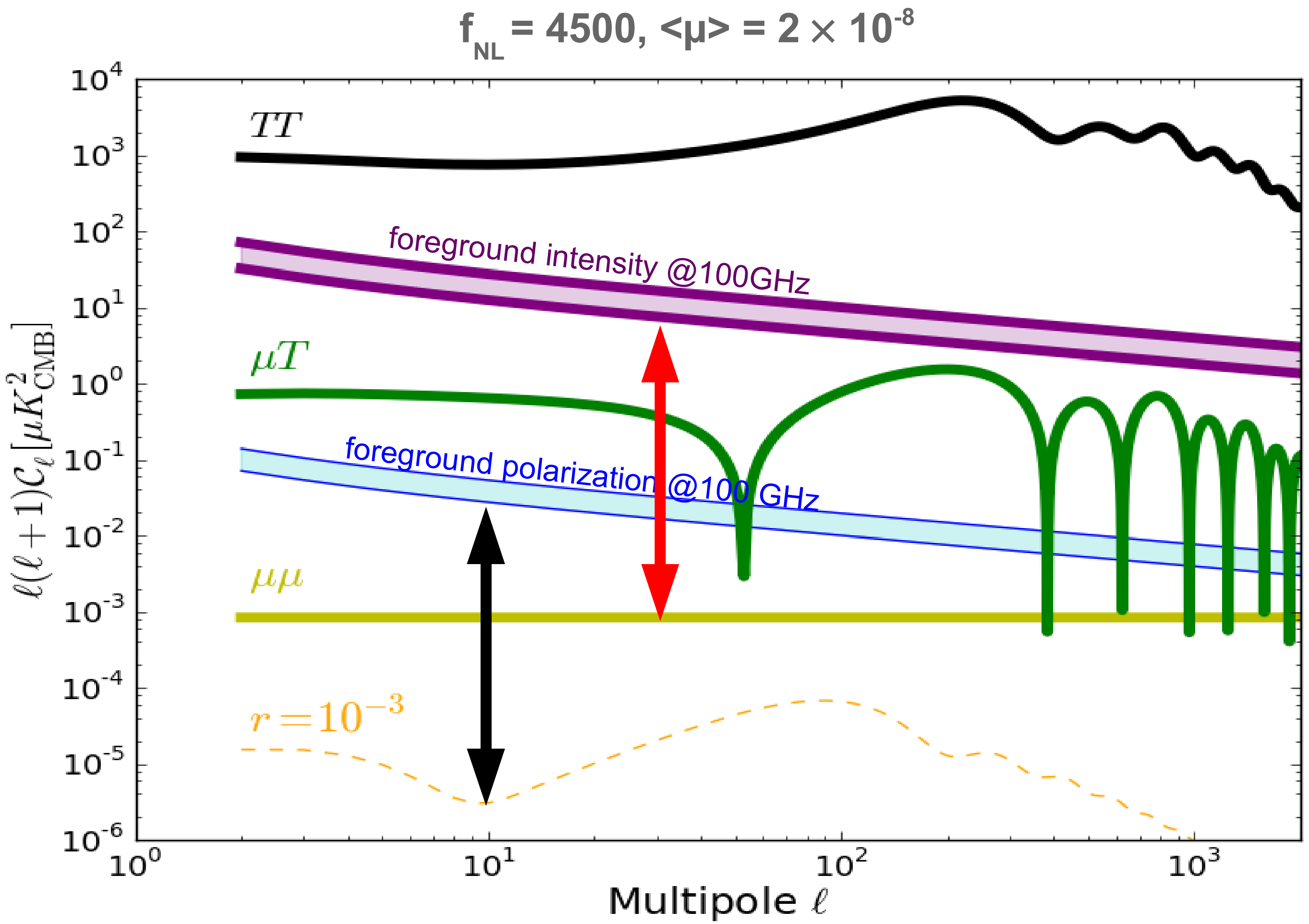

μ-T correlation signal between CMB temperature and μ-distortion anisotropies

→ *even more accessible signal, allowing to constrain $f_{NL}(k \approx 740\ \mathrm{Mpc}^{-1})$*

→ to be definitely considered by future CMB satellites...

Cosmic history of CMB spectral distortions

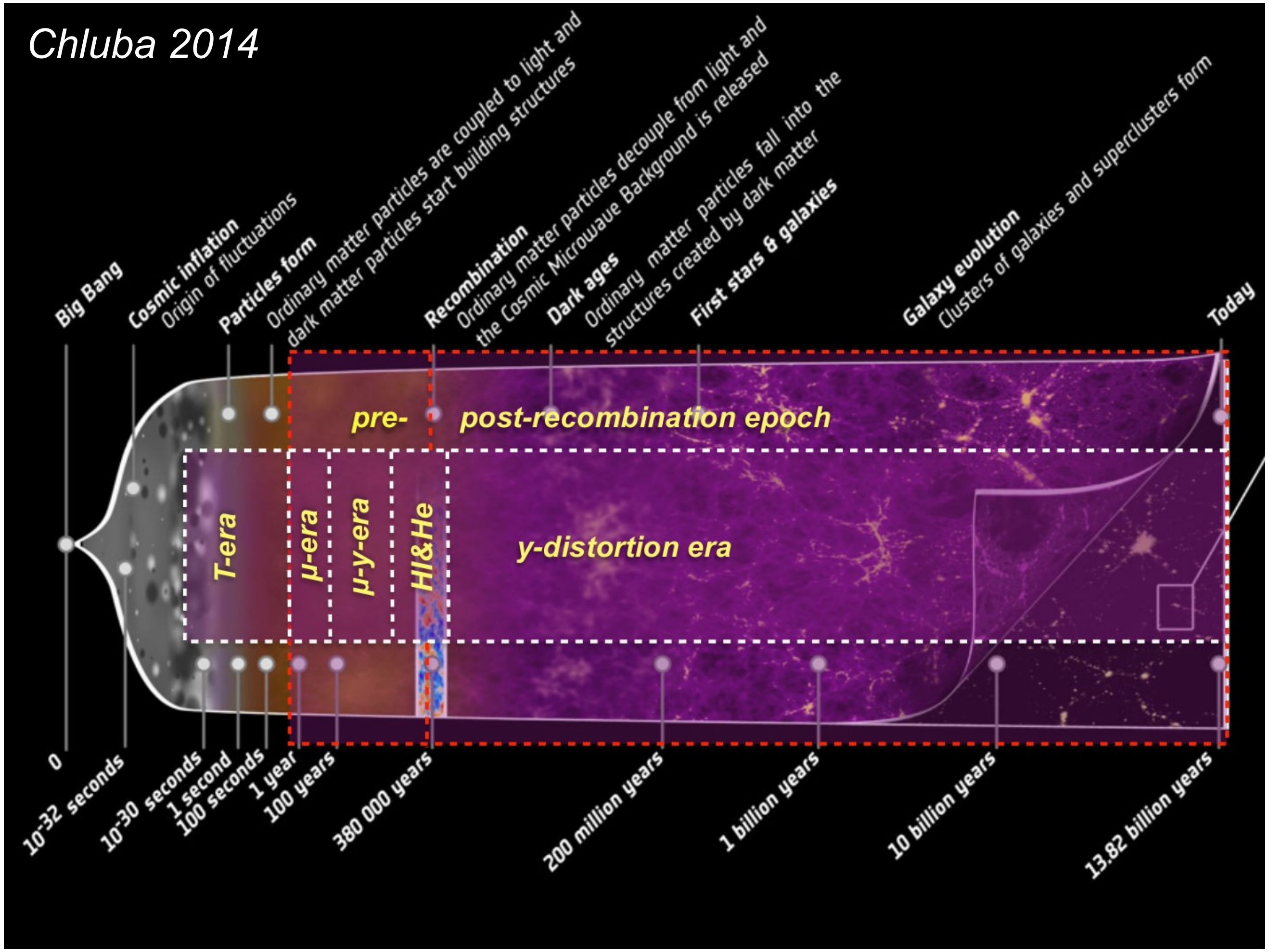

The problem of foregrounds

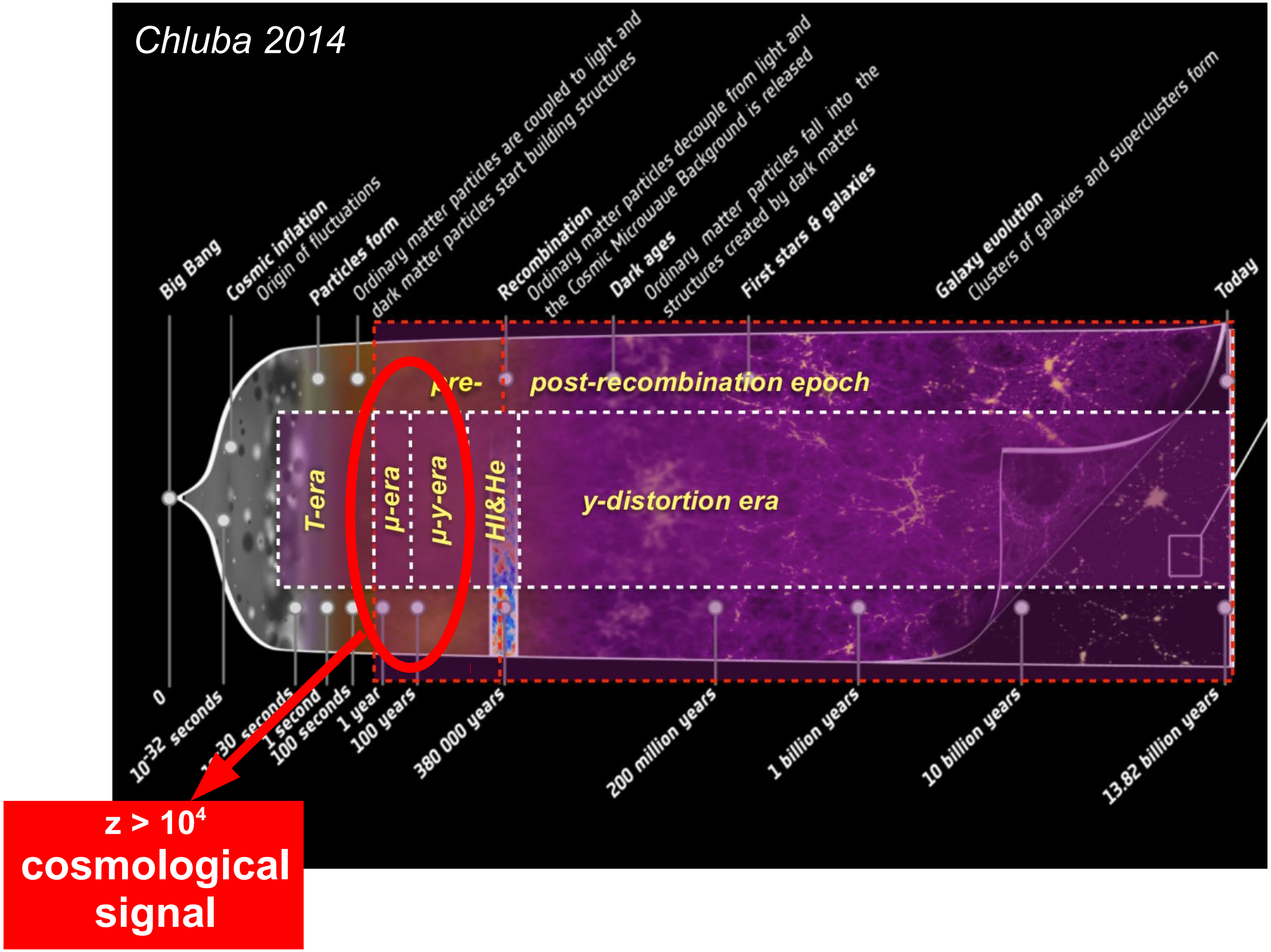

μ-type spectral distortions open a new window to probe physics occurring behind the last-scattering surface, where the universe is invisible!

The problem of foregrounds

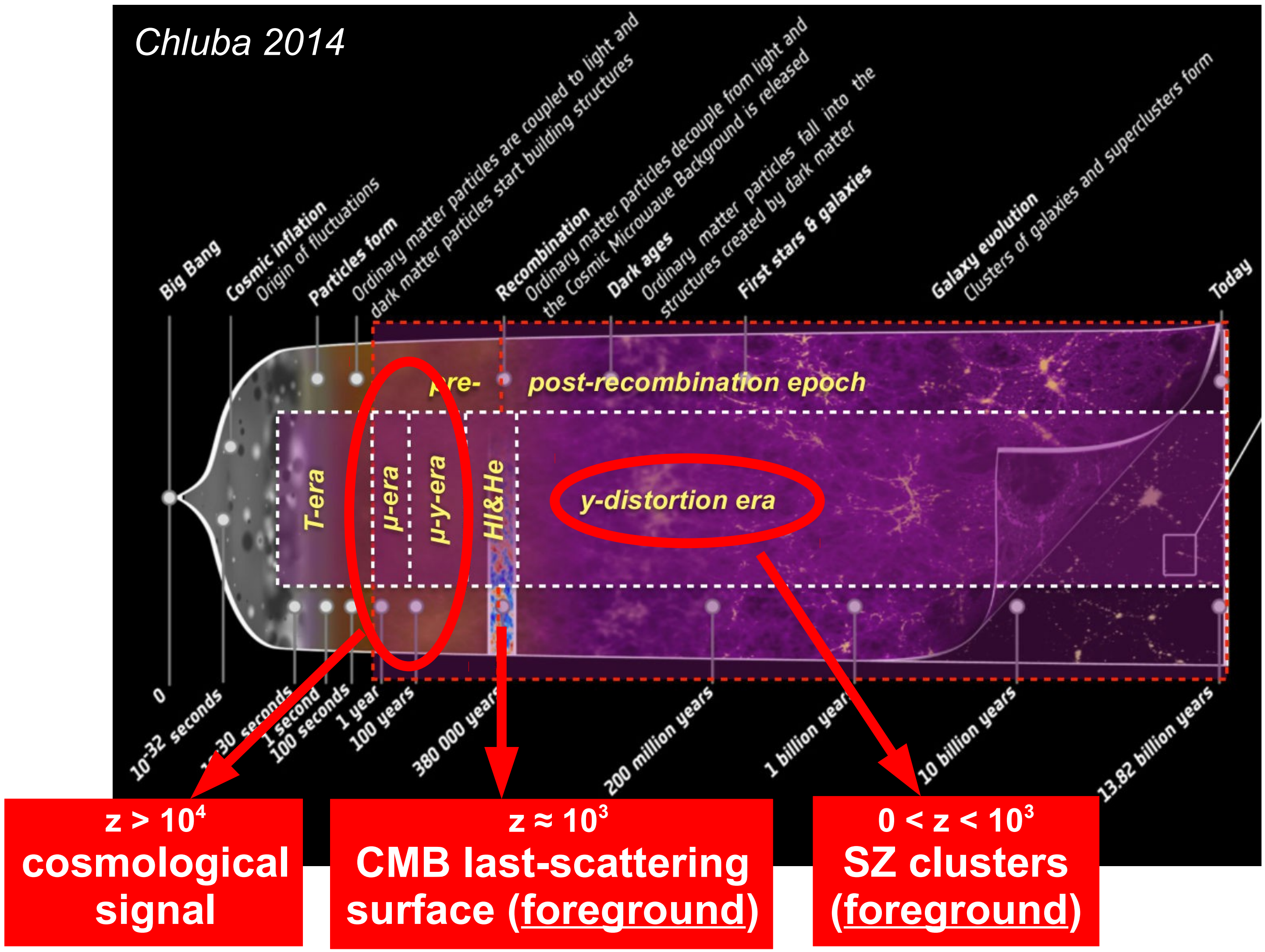

μ-type spectral distortions open a new window to probe physics occurring behind the last-scattering surface, where the universe is invisible!

The problem of foregrounds

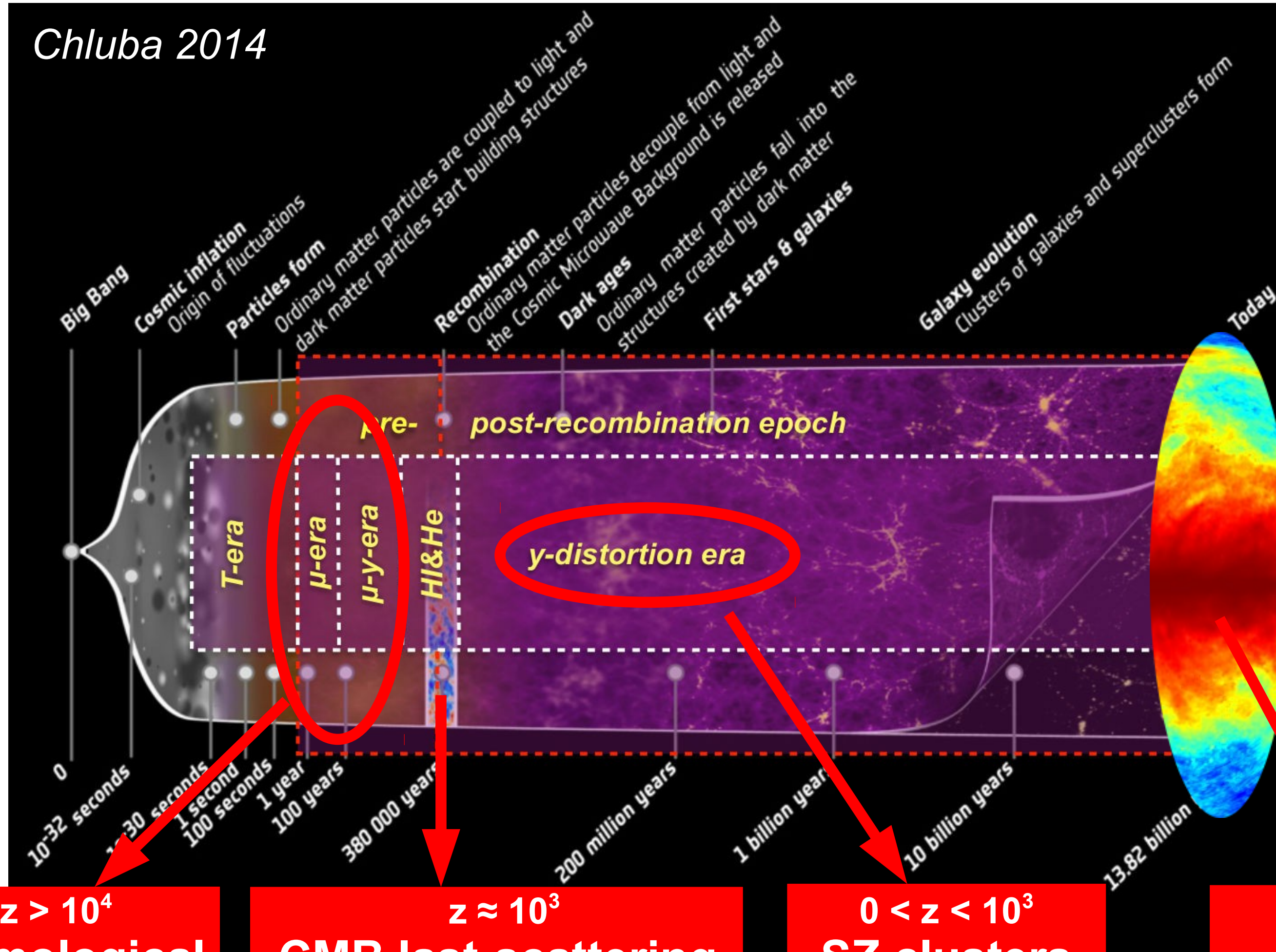

$z > 10^4$
cosmological signal

$z \approx 10^3$
CMB last-scattering surface (foreground)

$0 < z < 10^3$
SZ clusters (foreground)

$z = 0$
Galactic foregrounds

μ-type spectral distortions open a new window to probe physics occurring behind the last-scattering surface, where the universe is invisible!

Component separation : the problem

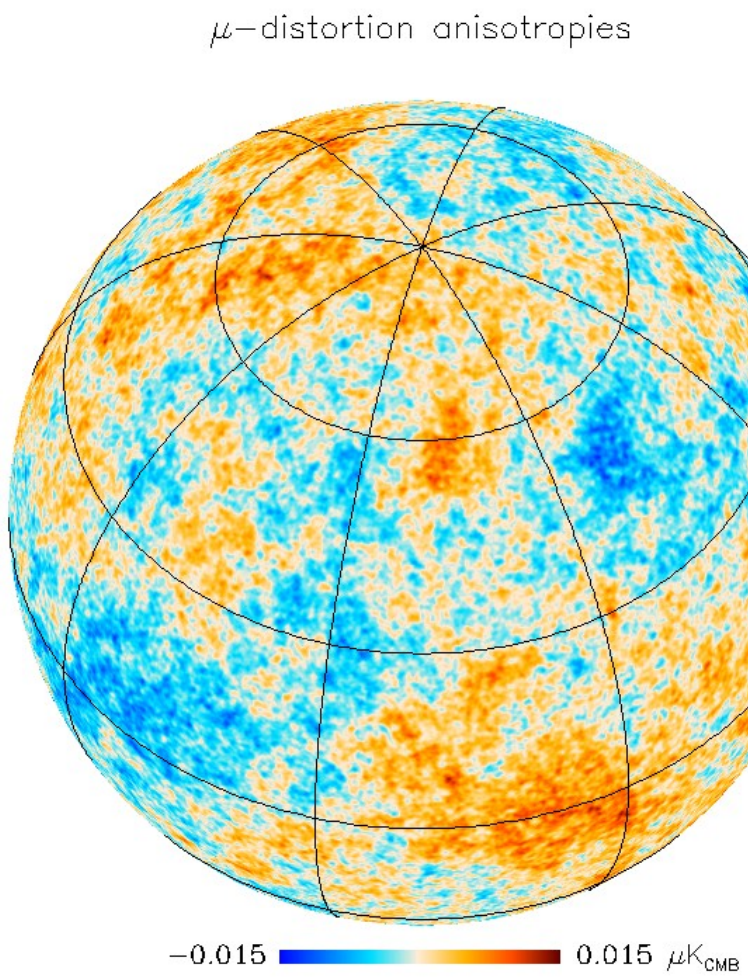

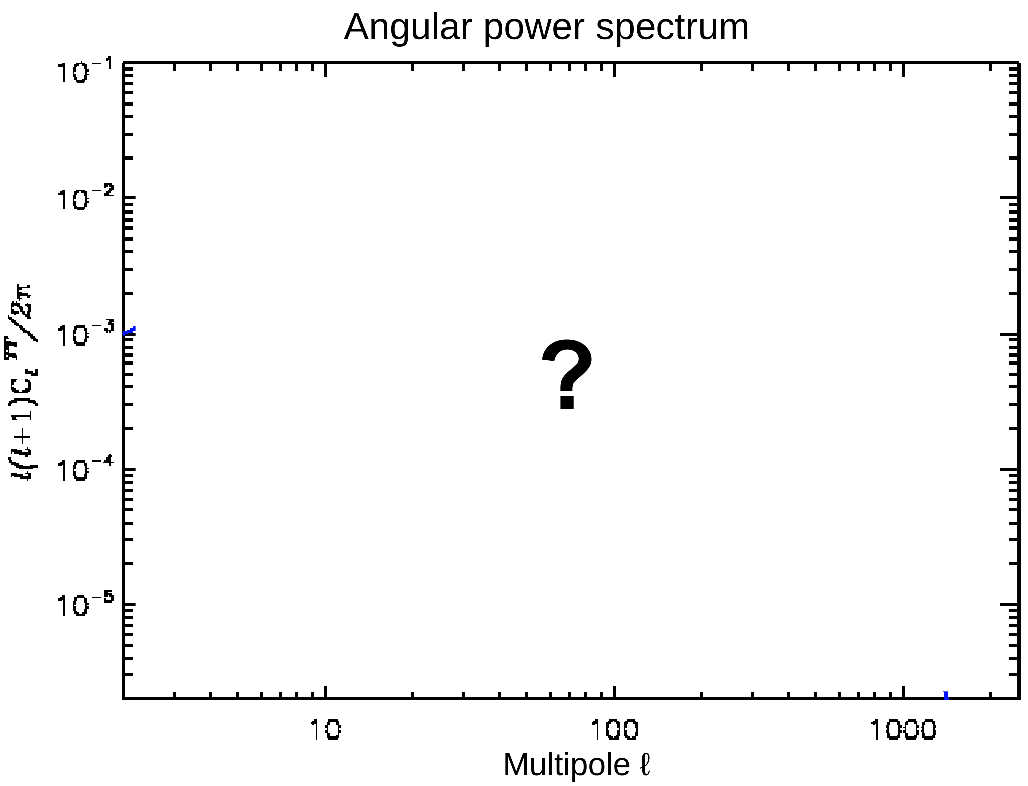

Component separation : the problem

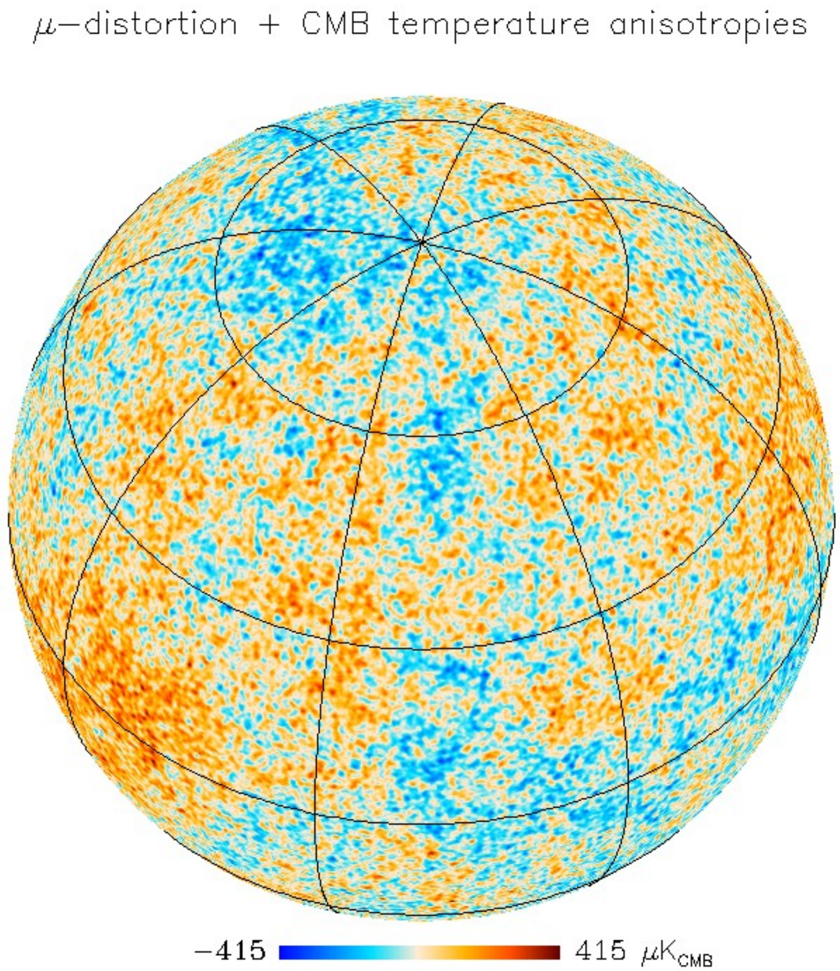

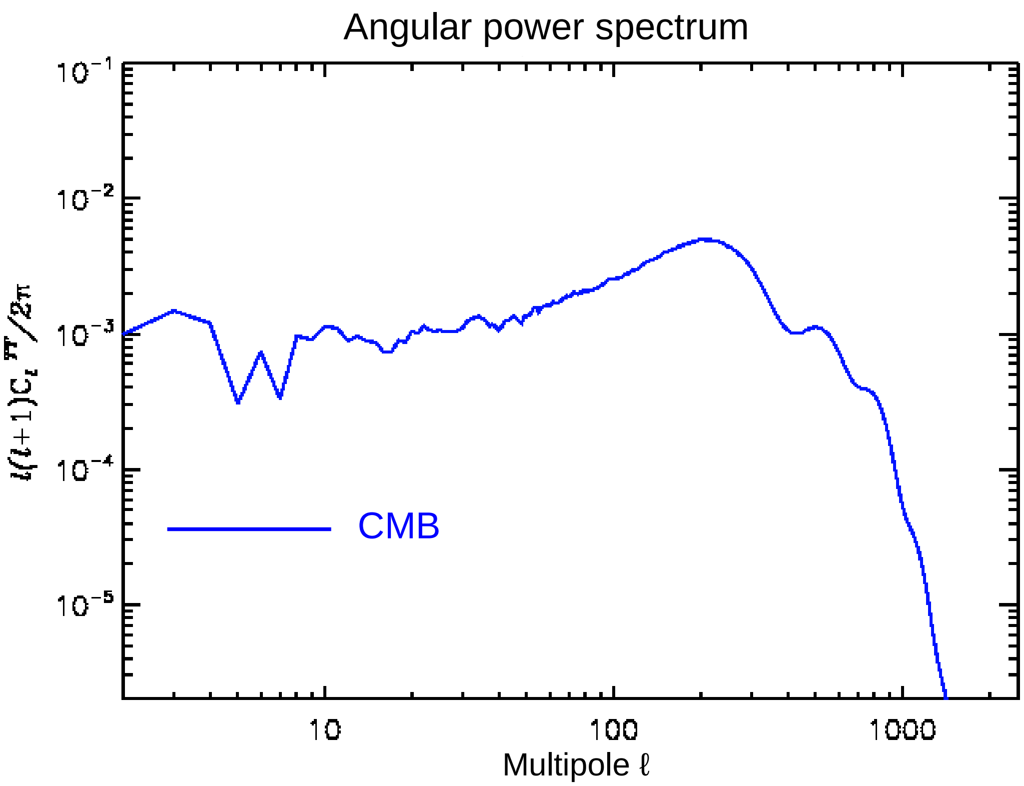

Component separation : the problem

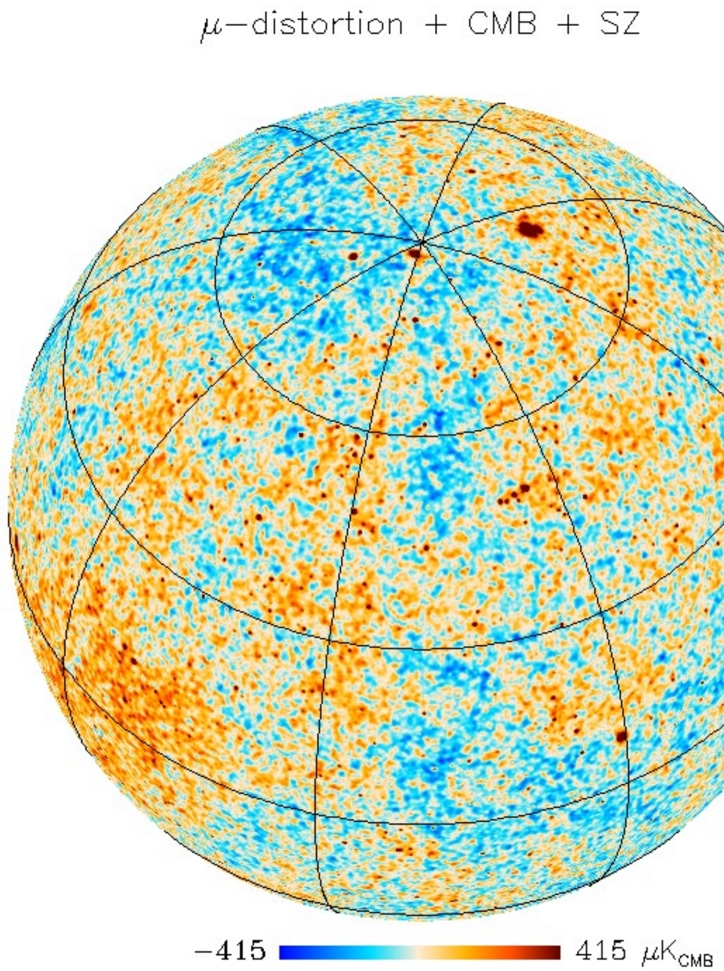

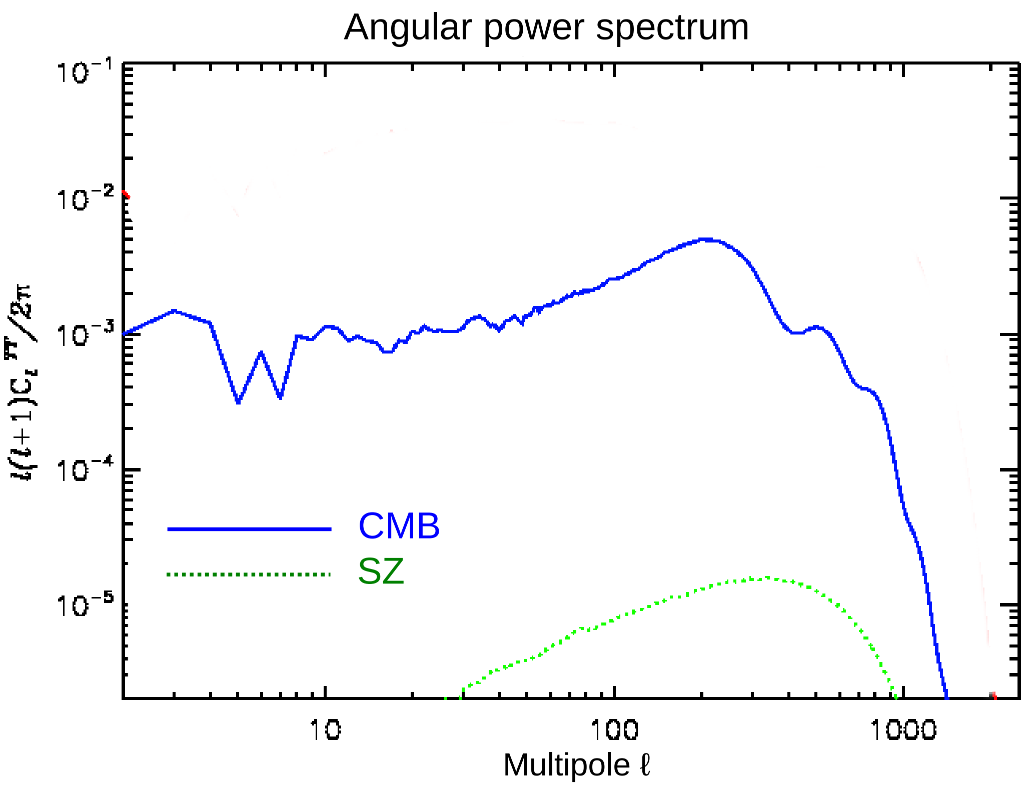

Component separation : the problem

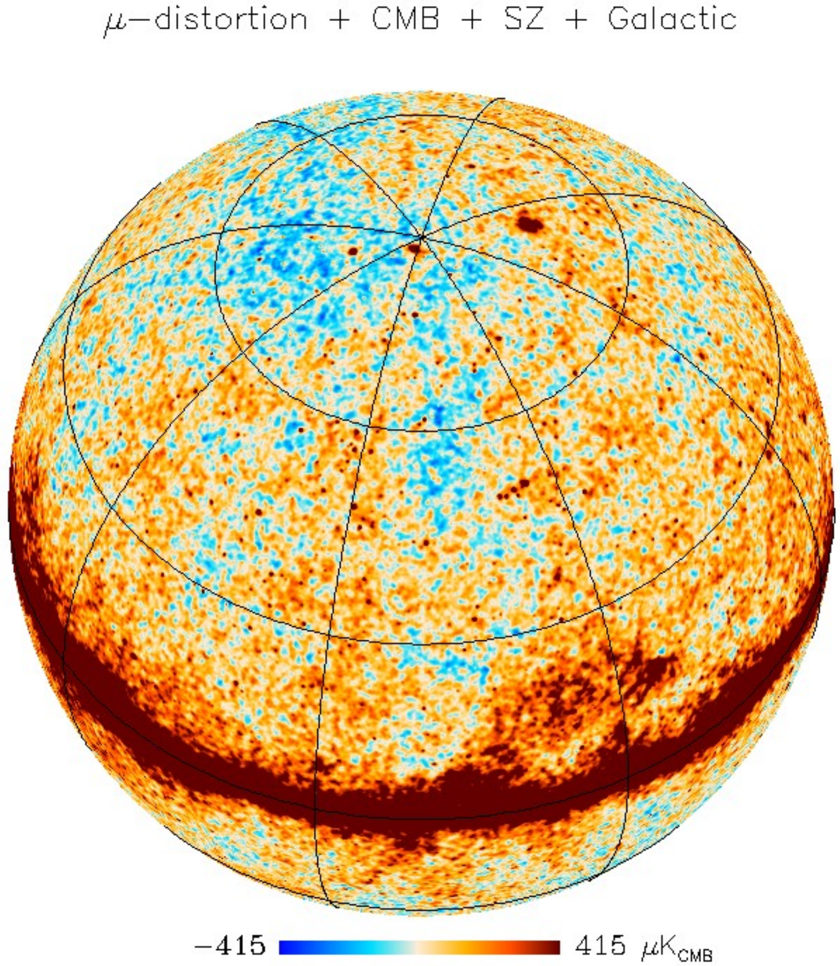

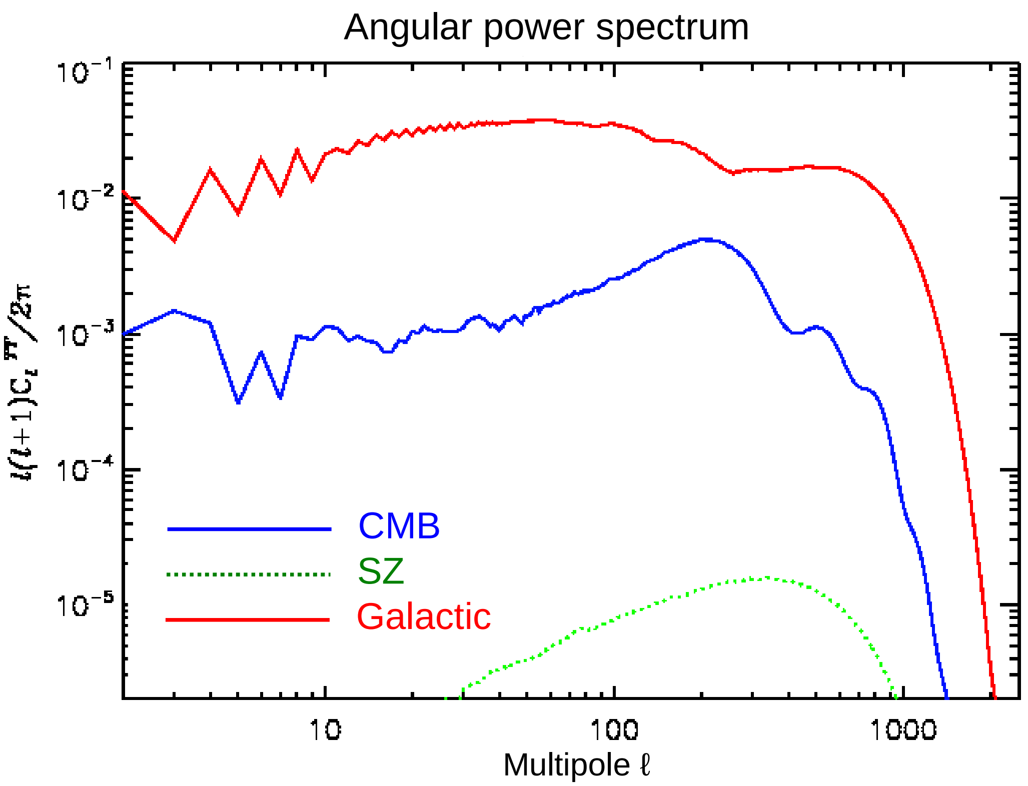

Component separation : the problem

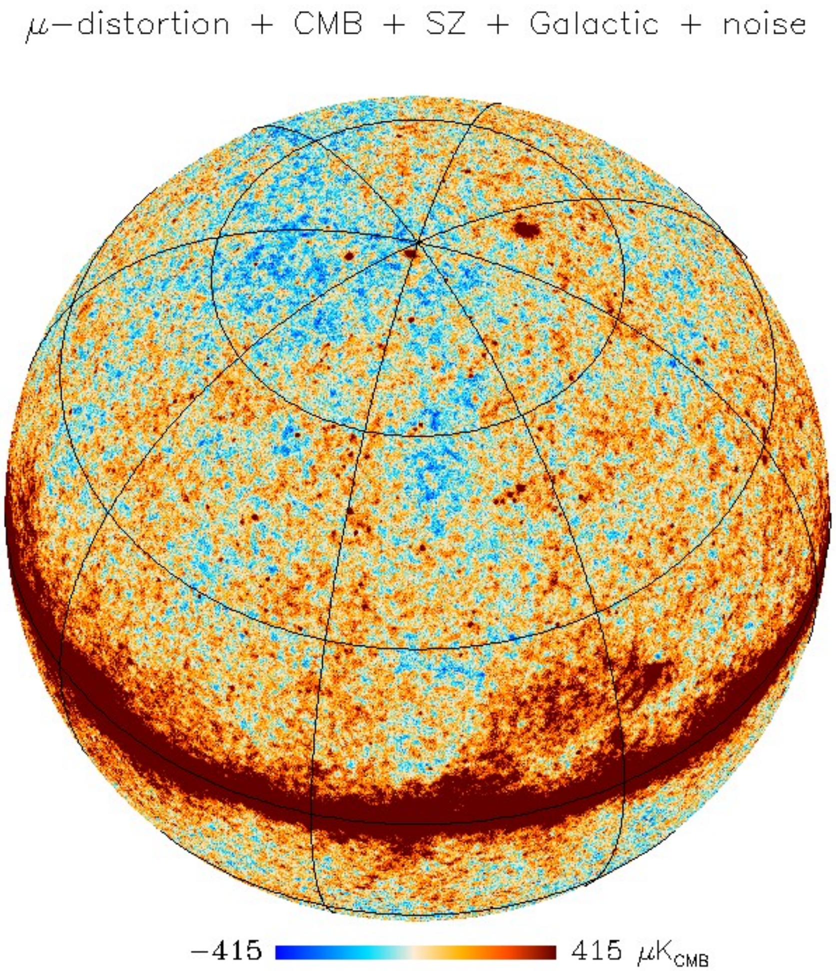

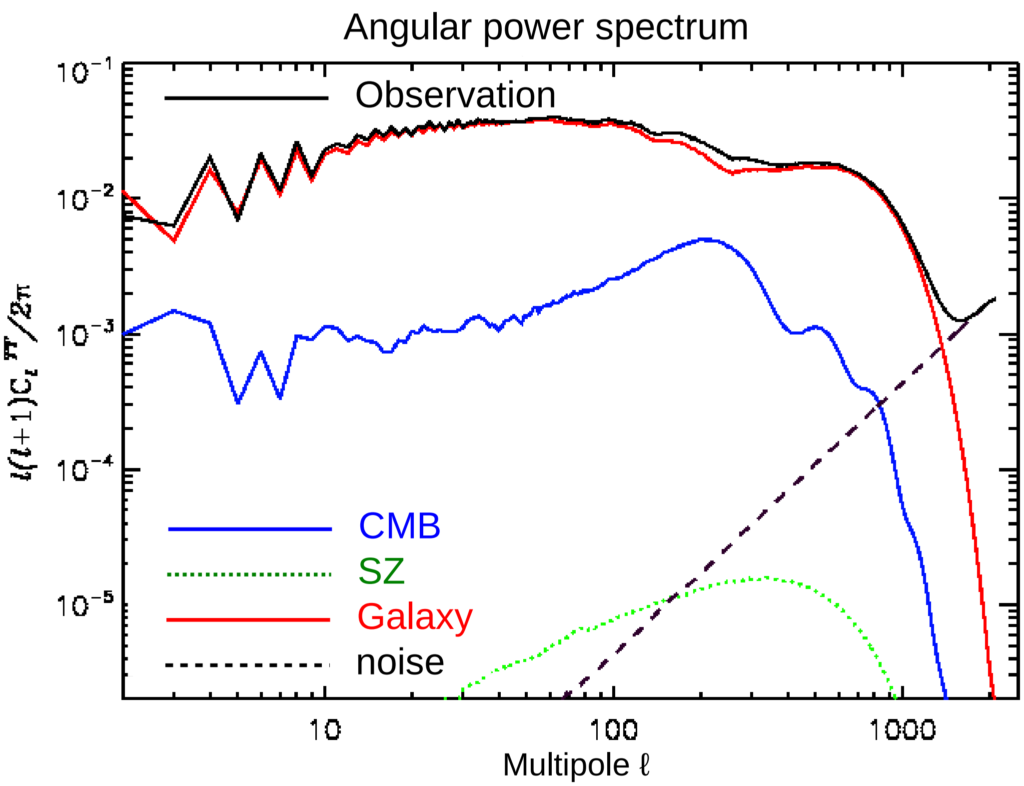

Standard ILC

Sky observation at frequency ν and pixel n

"foregrounds + noise"

$$X_\nu(n) = a_\nu S_{CMB}(n) + b_\nu S_{SZ}(n) + N_\nu(n)$$

spectral emission laws

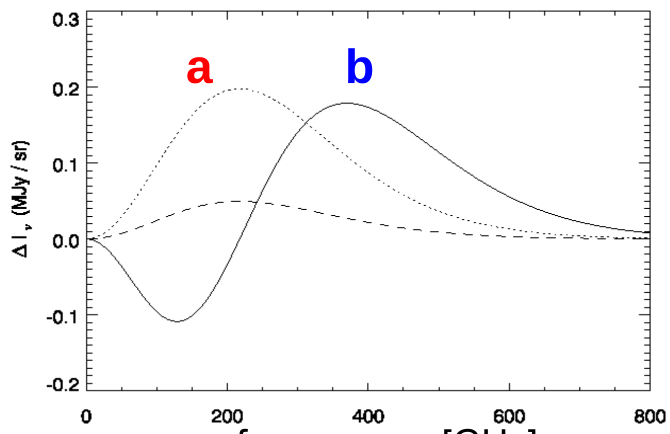

Minimum-variance weighted linear combination of the frequency maps:

$$\hat{S}_{CMB}(n) = \sum w_\nu X_\nu(n)$$

where $\begin{cases} \text{variance } \langle \hat{s}^2 \rangle \text{ minimum} \\ \sum w_\nu a_\nu = 1 \end{cases}$

CMB reconstruction

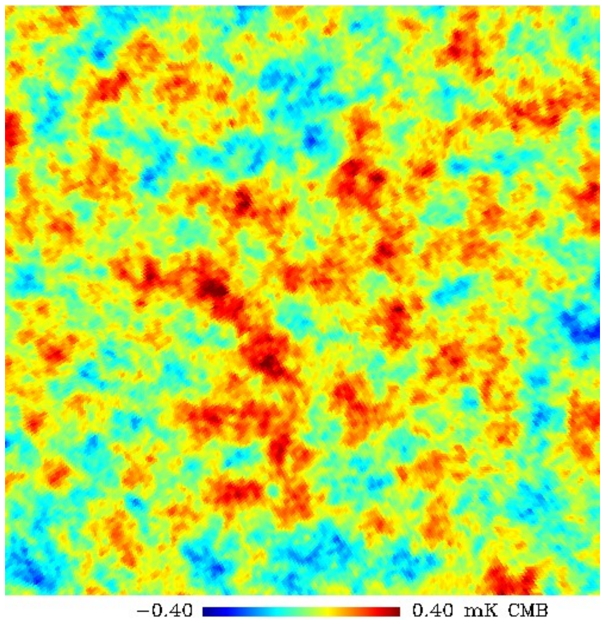

standard ILC

$$\boxed{W = \frac{a^t C^{-1}}{a^t C^{-1} a}}$$

Benett et al, 2003
Tegmark et al, 2003
Eriksen et al, 2004
Delabrouille et al, 2009

Standard ILC

Sky observation at frequency ν and pixel n

“foregrounds + noise”

$$X_\nu(n) = a_\nu S_{CMB}(n) + b_\nu S_{SZ}(n) + N_\nu(n)$$

spectral emission laws

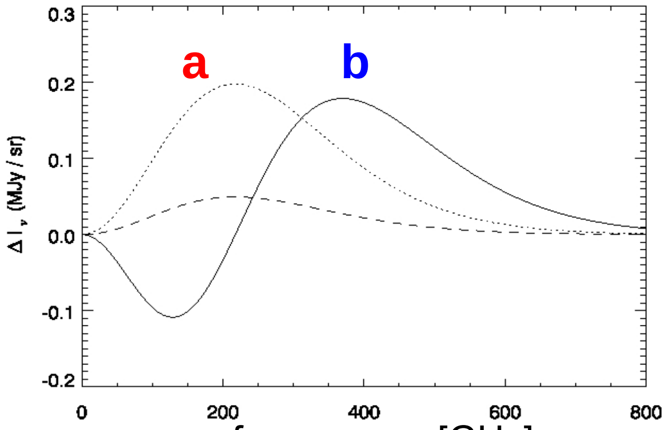

Minimum-variance weighted linear combination of the frequency maps:

$$\hat{s}_{SZ}(n) = \sum w_\nu X_\nu(n)$$

where
$$\begin{cases} \text{variance } \langle \hat{s}^2 \rangle \text{ minimum} \\ \sum w_\nu b_\nu = 1 \end{cases}$$

SZ reconstruction

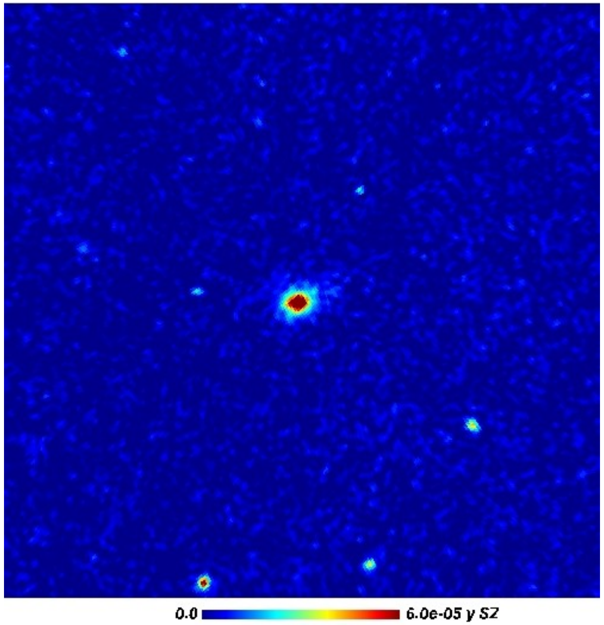

standard ILC

$$\boxed{W = \frac{b^t C^{-1}}{b^t C^{-1} b}}$$

Benett et al, 2003
Tegmark et al, 2003
Eriksen et al, 2004
Delabrouille et al, 2009

Constrained ILC

Sky observation at frequency ν and pixel n

"foregrounds + noise"

$$X_\nu(n) = a_\nu S_{CMB}(n) + b_\nu S_{SZ}(n) + N_\nu(n)$$

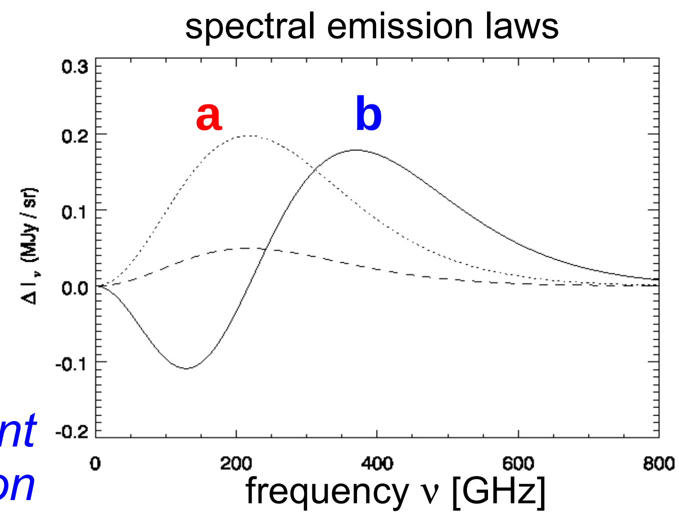

$$\hat{s}_{CMB}(n) = \sum w_\nu X_\nu(n)$$

$$\text{where} \begin{cases} \text{variance } \langle \hat{s}^2 \rangle \text{ minimum} \\ \sum w_\nu a_\nu = 1 \\ \sum w_\nu b_\nu = 0 \end{cases}$$

orthogonality constraint to kill SZ contamination

SZ-free CMB reconstruction

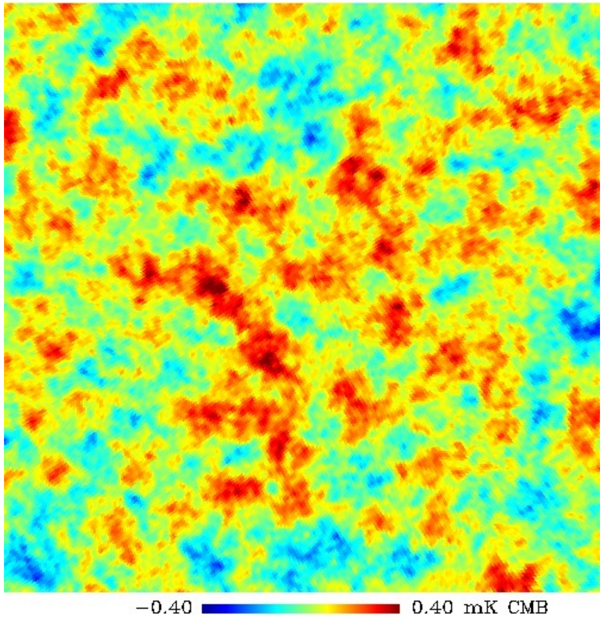

Constrained ILC

$$\boxed{W = \frac{(b^t C^{-1} b)\, a^t C^{-1} - (a^t C^{-1} a)\, b^t C^{-1}}{(a^t C^{-1} a)(b^t C^{-1} b) - (a^t C^{-1} b)^2}}$$

Remazeilles, Delabrouille, Cardoso, MNRAS (2011)

Standard ILC

input thermal SZ

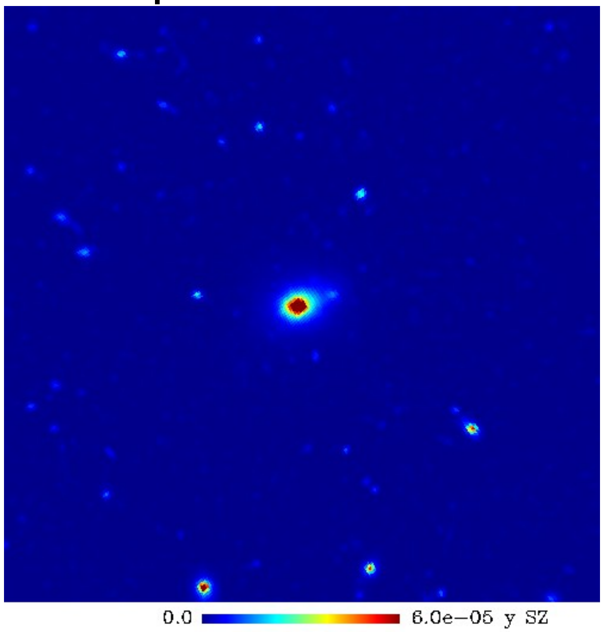

input kinetic SZ

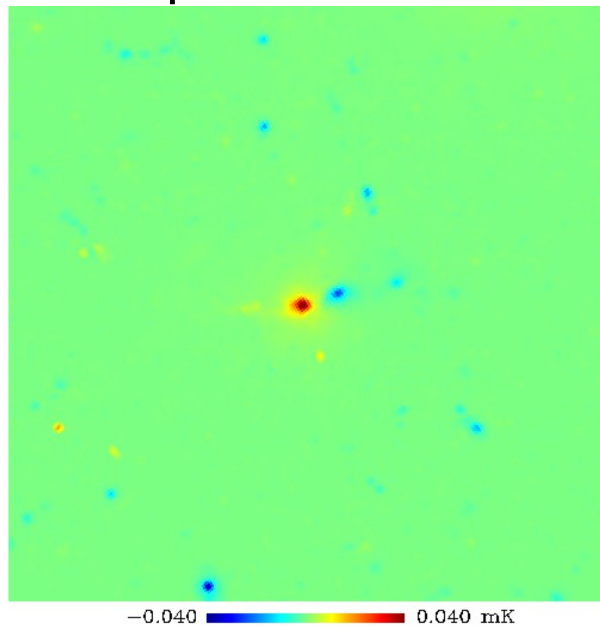

input CMB

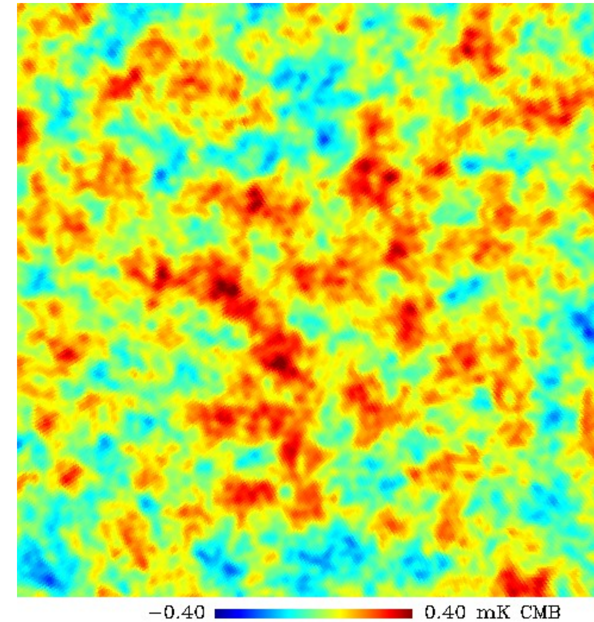

ILC

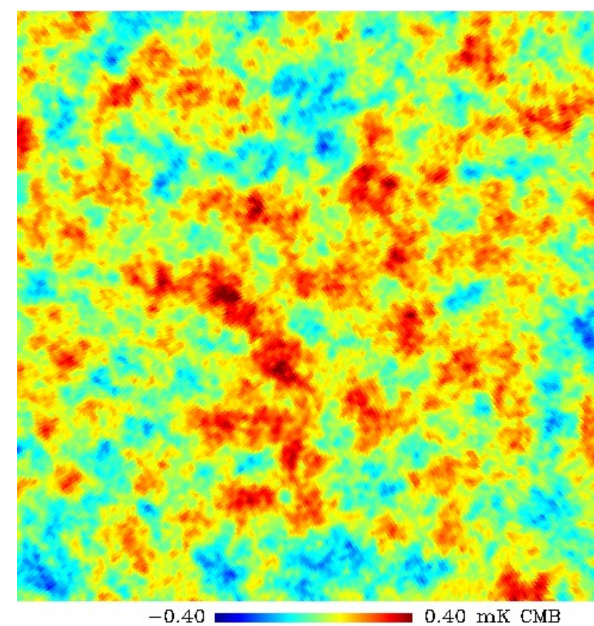

$$\mathbf{w} = \frac{\mathbf{a}^t \mathbf{C}^{-1}}{\mathbf{a}^t \mathbf{C}^{-1} \mathbf{a}}$$

Bennett et al (2003), Tegmark et al (2003)
Eriksen et al (2004), Delabrouille et al (2009)

Standard ILC

input thermal SZ

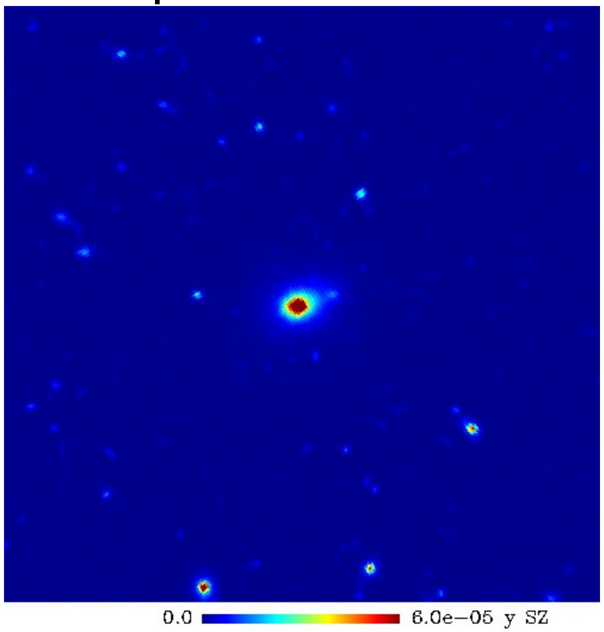

input kinetic SZ

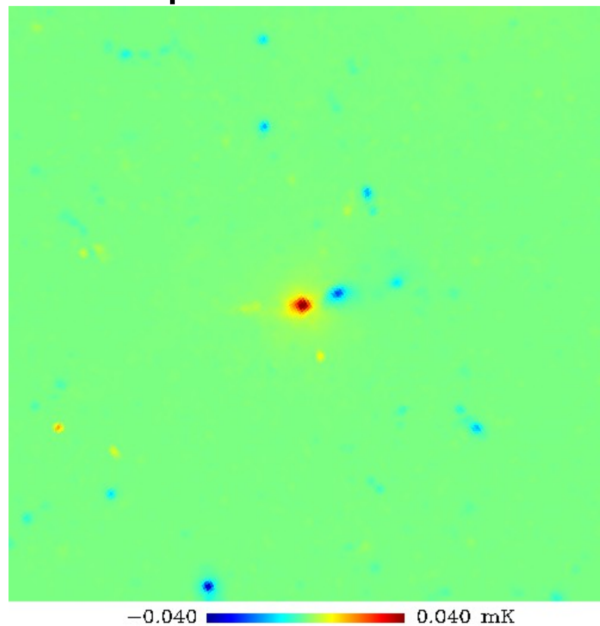

input CMB

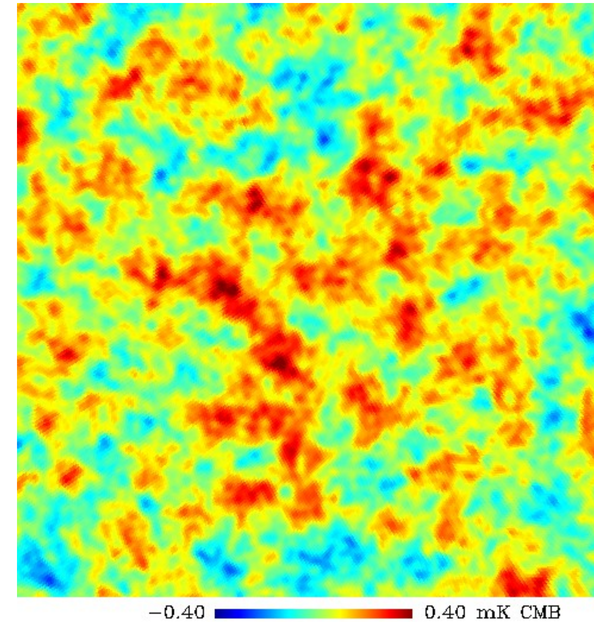

error: ILC - CMB

Thermal SZ rediduals !
(clusters in the CMB)

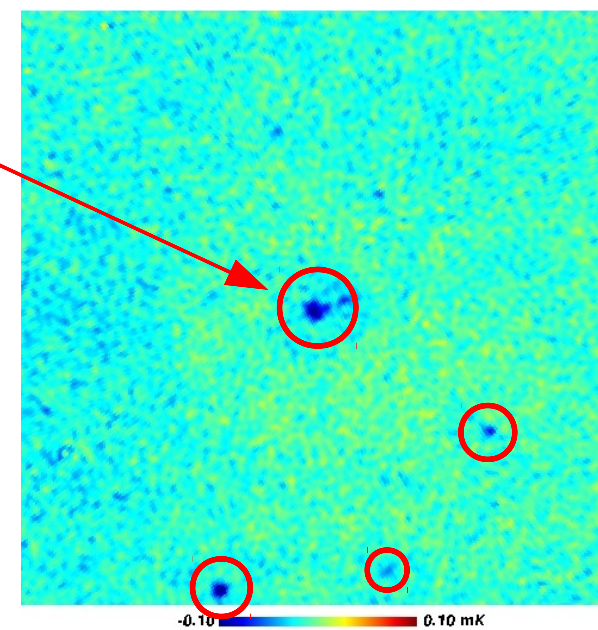

$$\mathbf{w} = \frac{\mathbf{a}^t \mathbf{C}^{-1}}{\mathbf{a}^t \mathbf{C}^{-1} \mathbf{a}}$$

Bennett et al (2003), Tegmark et al (2003)
Eriksen et al (2004), Delabrouille et al (2009)

Constrained ILC

input thermal SZ

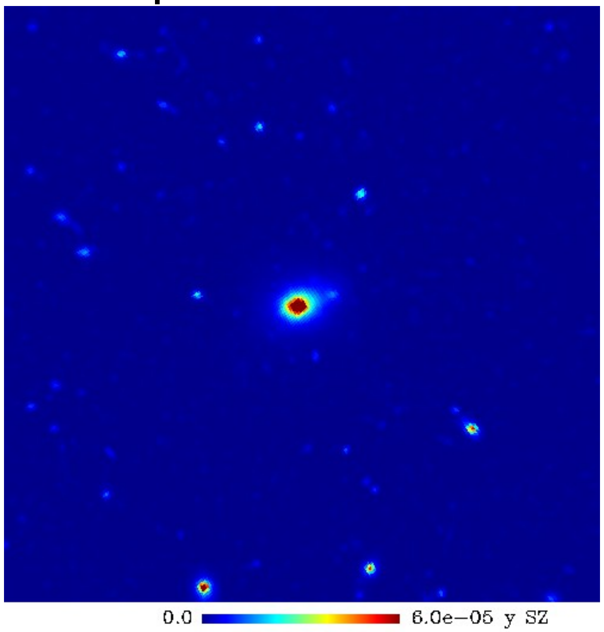

input kinetic SZ

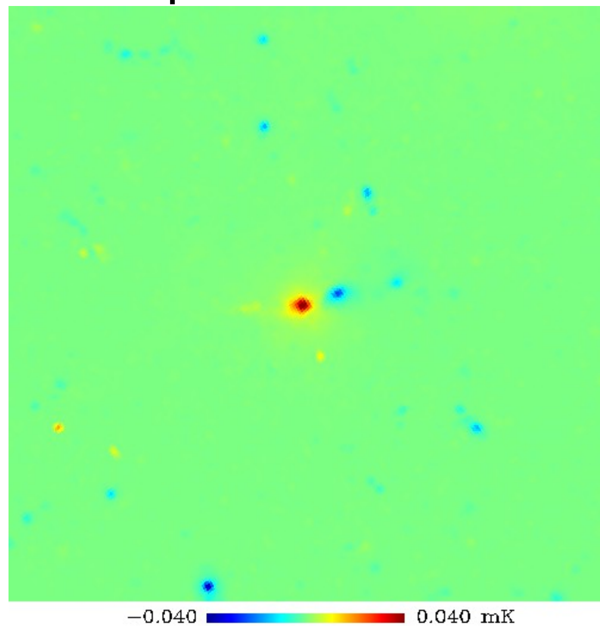

input CMB

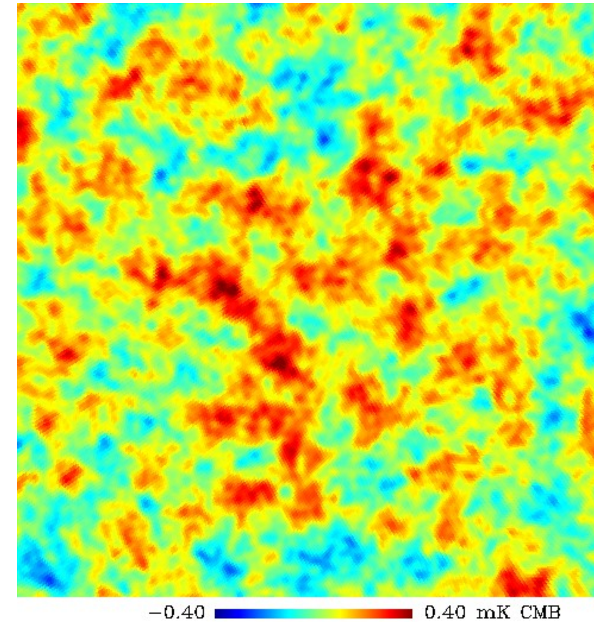

error: Constrained ILC - CMB

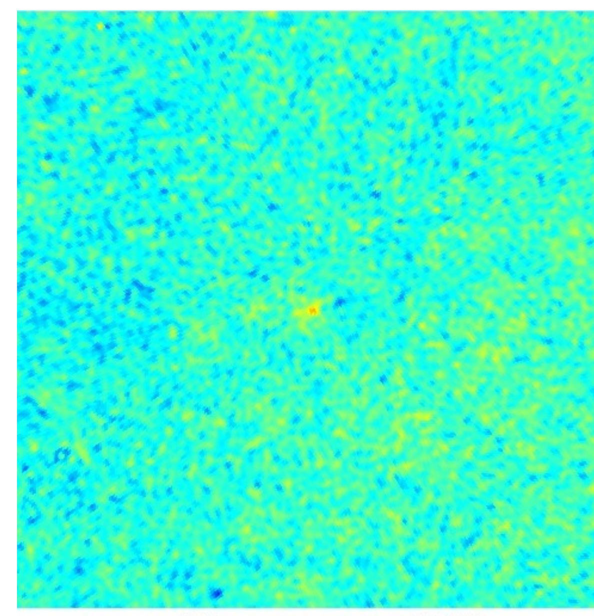

$$w = \frac{(b^t C^{-1} b)\; a^t C^{-1} - (a^t C^{-1} a)\; b^t C^{-1}}{(a^t C^{-1} a)\,(b^t C^{-1} b) - (a^t C^{-1} b)^2}$$

Remazeilles, Delabrouille, Cardoso, MNRAS (2011)

Extracting foreground-obscured μ-anisotropies

$$\text{data}(\nu;n) = \mu + T + (\text{foregrounds+noise})$$

sky observation at frequency ν and pixel n

μ-distortion anisotropies

CMB temperature anisotropies

- *CMB **T** anisotropies is a significant foreground to **μ**-distortion anisotropies*
- *Most sneaky, the CMB **T** foreground is also correlated with the **μ** signal!*
- *If residual **T** anisotropies are left in the reconstructed **μ**-distortion signal after component separation*

$$\hat{\mu} = \mu + \varepsilon_1 T + \varepsilon_2 (\text{foregrounds+noise})$$

*then the **μ-T correlation signal** will be biased by **spurious TT correlations:***

$$\hat{\mu} \times \hat{T} = \mu \times T + \varepsilon_1 TT + \ldots$$

Remazeilles & Chluba (2018)** → **our solution: use the “Constrained ILC” approach

CMB-free μ-distortion reconstruction

$$X(\nu;n) = a_\mu(\nu)\,\mu(n) + a_T(\nu)\,T(n) + N(\nu;n)$$

sky observation at frequency ν and pixel n

μ SED

μ-distortion anisotropies

CMB SED

CMB temperature anisotropies

foregrounds + noise

Constrained ILC estimate:

$$\hat{\mu}(n) = \sum_\nu w(\nu)\, X(\nu;n)$$

such that

$$\begin{cases} \text{variance } \langle \mu^2 \rangle \text{ minimum} & (1) \\ \sum w_\nu\, a_\mu(\nu) = 1 & (2) \\ \sum w_\nu\, a_T(\nu) = 0 & (3) \end{cases}$$

orthogonality constraint to kill CMB T contamination

Remazeilles & Chluba (2018)

CMB-free μ-distortion reconstruction

$$X(\nu;n) = a_\mu(\nu)\,\mu(n) + a_T(\nu)\,T(n) + N(\nu;n)$$

- $X(\nu;n)$: sky observation at frequency ν and pixel n
- $a_\mu(\nu)$: μ SED
- $\mu(n)$: **μ-distortion anisotropies**
- $a_T(\nu)$: CMB SED
- $T(n)$: CMB temperature anisotropies
- $N(\nu;n)$: foregrounds + noise

Constrained ILC estimate:

$$\hat{\mu}(n) = \sum_\nu w(\nu)\, X(\nu;n)$$

such that
$$\begin{cases} \text{variance } \langle\mu^2\rangle \text{ minimum} & (1) \\ \sum w_\nu\, a_\mu(\nu) = 1 & (2) \\ \sum w_\nu\, a_T(\nu) = 0 & (3) \end{cases}$$

(3) → *orthogonality constraint to kill CMB T contamination*

$$\hat{\mu}(n) = \underbrace{\left(\sum w_\nu\, a_\mu(\nu)\right)}_{\substack{=1 \\ (2)}} \mu + \underbrace{\left(\sum w_\nu\, a_T(\nu)\right)}_{\substack{=0 \\ (3)}} T + \underbrace{\sum w_\nu N_\nu}_{\substack{\text{minimized} \\ (1)}}$$

Remazeilles & Chluba (2018)

CMB-free μ-distortion reconstruction

$$X(\nu;n) \;=\; a_\mu(\nu)\,\mu(n) \;+\; a_T(\nu)\,T(n) \;+\; N(\nu;n)$$

sky observation at frequency ν and pixel n

μ SED

μ-distortion anisotropies

CMB SED

CMB temperature anisotropies

foregrounds + noise

Constrained ILC estimate:

$$\hat{\mu}(n) \;=\; \sum_\nu w(\nu)\, X(\nu;n)$$

$$\text{such that} \begin{cases} \text{variance } \langle \mu^2 \rangle \text{ minimum} & (1) \\ \sum_\nu w_\nu\, a_\mu(\nu) = 1 & (2) \\ \sum_\nu w_\nu\, a_T(\nu) = 0 & (3) \end{cases}$$

orthogonality constraint to kill CMB T contamination

$$\hat{\mu}(n) = \underbrace{\left(\sum_\nu w_\nu\, a_\mu(\nu) \right)}_{\substack{= 1 \\ (2)}} \mu + \cancel{\underbrace{\left(\sum_\nu w_\nu\, a_T(\nu) \right)}_{\substack{= 0 \\ (3)}}}\, T + \underbrace{\sum_\nu w_\nu N_\nu}_{\substack{\text{minimized} \\ (1)}}$$

Remazeilles & Chluba (2018)

CMB-free μ-distortion reconstruction

$$X(\nu;n) = a_\mu(\nu)\,\mu(n) + a_T(\nu)\,T(n) + N(\nu;n)$$

- $X(\nu;n)$: sky observation at frequency ν and pixel n
- $a_\mu(\nu)$: μ SED
- $\mu(n)$: **μ-distortion anisotropies**
- $a_T(\nu)$: CMB SED
- $T(n)$: CMB temperature anisotropies
- $N(\nu;n)$: foregrounds + noise

Constrained ILC estimate:

$$\hat{\mu}(n) = \sum_\nu w(\nu)\, X(\nu;n)$$

such that

$$\begin{cases} \text{variance } \langle\mu^2\rangle \text{ minimum} & (1) \\ \sum w_\nu\, a_\mu(\nu) = 1 & (2) \\ \sum w_\nu\, a_T(\nu) = 0 & (3) \end{cases}$$

(3) → *orthogonality constraint to kill CMB T contamination*

$$\rightarrow \hat{\mu} \times \hat{T} = \mu \times T + \cancel{\varepsilon_1 TT} + \ldots$$

Remazeilles & Chluba (2018)

CMB-free μ-distortion reconstruction

$$X(\nu;n) = a_\mu(\nu)\,\mu(n) + a_T(\nu)\,T(n) + N(\nu;n)$$

sky observation at frequency ν and pixel n

μ SED

<u>μ-distortion anisotropies</u>

CMB SED

CMB temperature anisotropies

foregrounds + noise

<u>Constrained ILC estimate</u>:

$$\hat{\mu}(n) = \sum_\nu w(\nu)\, X(\nu;n)$$

such that
$$\begin{cases} \text{variance } \langle\mu^2\rangle \text{ minimum} & (1) \\ \sum w_\nu\, a_\mu(\nu) = 1 & (2) \\ \sum w_\nu\, a_T(\nu) = 0 & (3) \end{cases}$$

orthogonality constraint to kill CMB T contamination

<u>Solution</u>:

$$\boxed{W = \frac{(a_T^t\, C^{-1}\, a_T)\, a_\mu^t\, C^{-1} - (a_\mu^t\, C^{-1}\, a_\mu)\, a_t^t\, C^{-1}}{(a_\mu^t\, C^{-1}\, a_\mu)(a_T^t\, C^{-1}\, a_T) - (a_\mu^t\, C^{-1}\, a_T)^2}}$$

Remazeilles & Chluba (2018)

Simulation of correlated μ and T fields

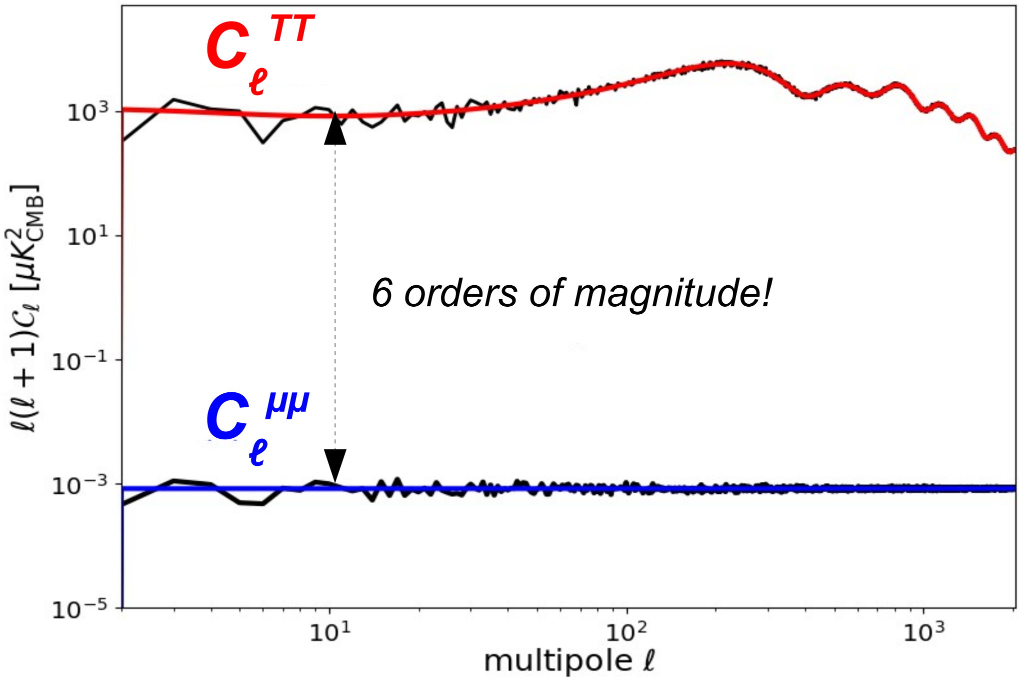

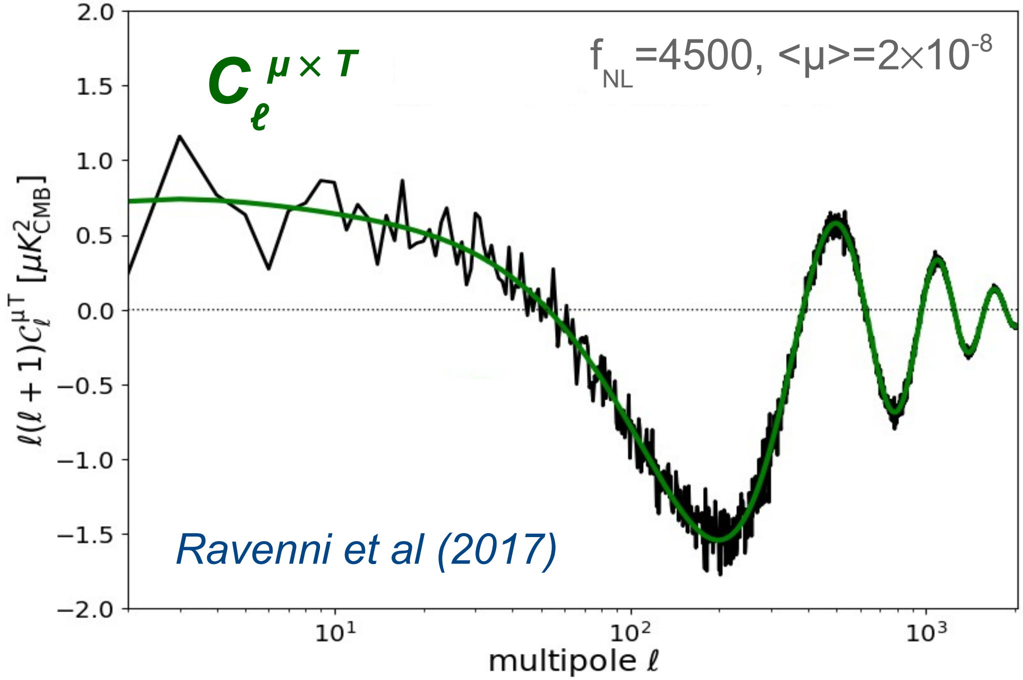

Remazeilles & Chluba (2018)

Simulation of correlated μ and T fields

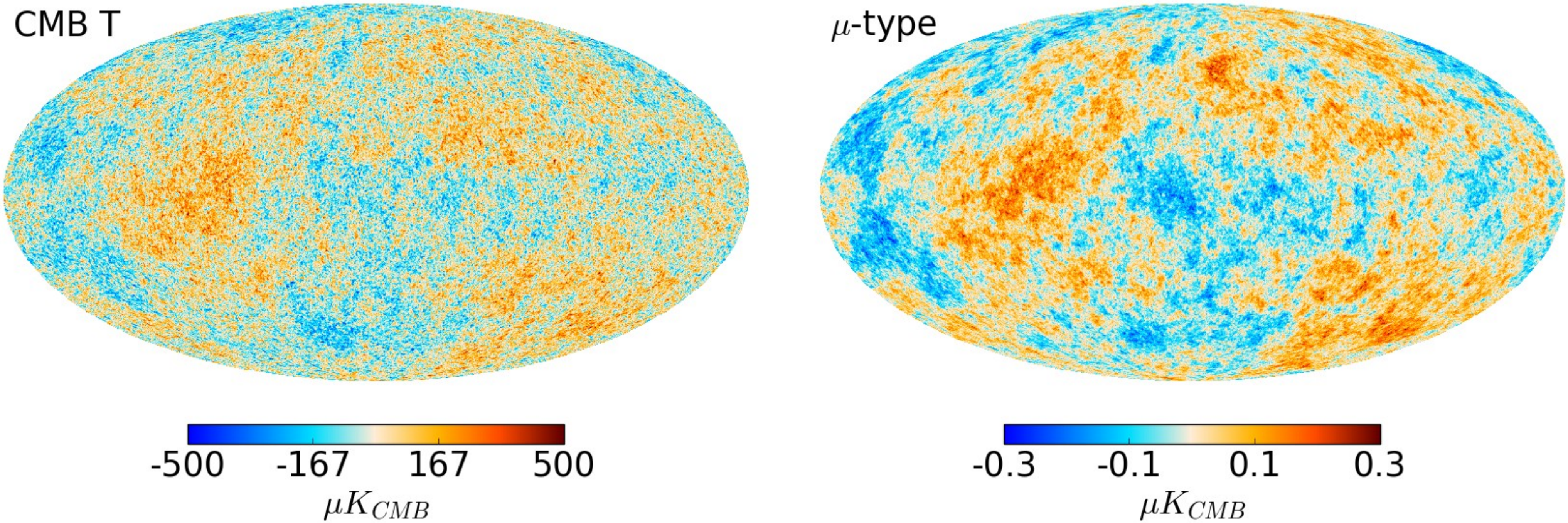

Remazeilles & Chluba (2018)

Our sky simulations (e.g. LiteBIRD)

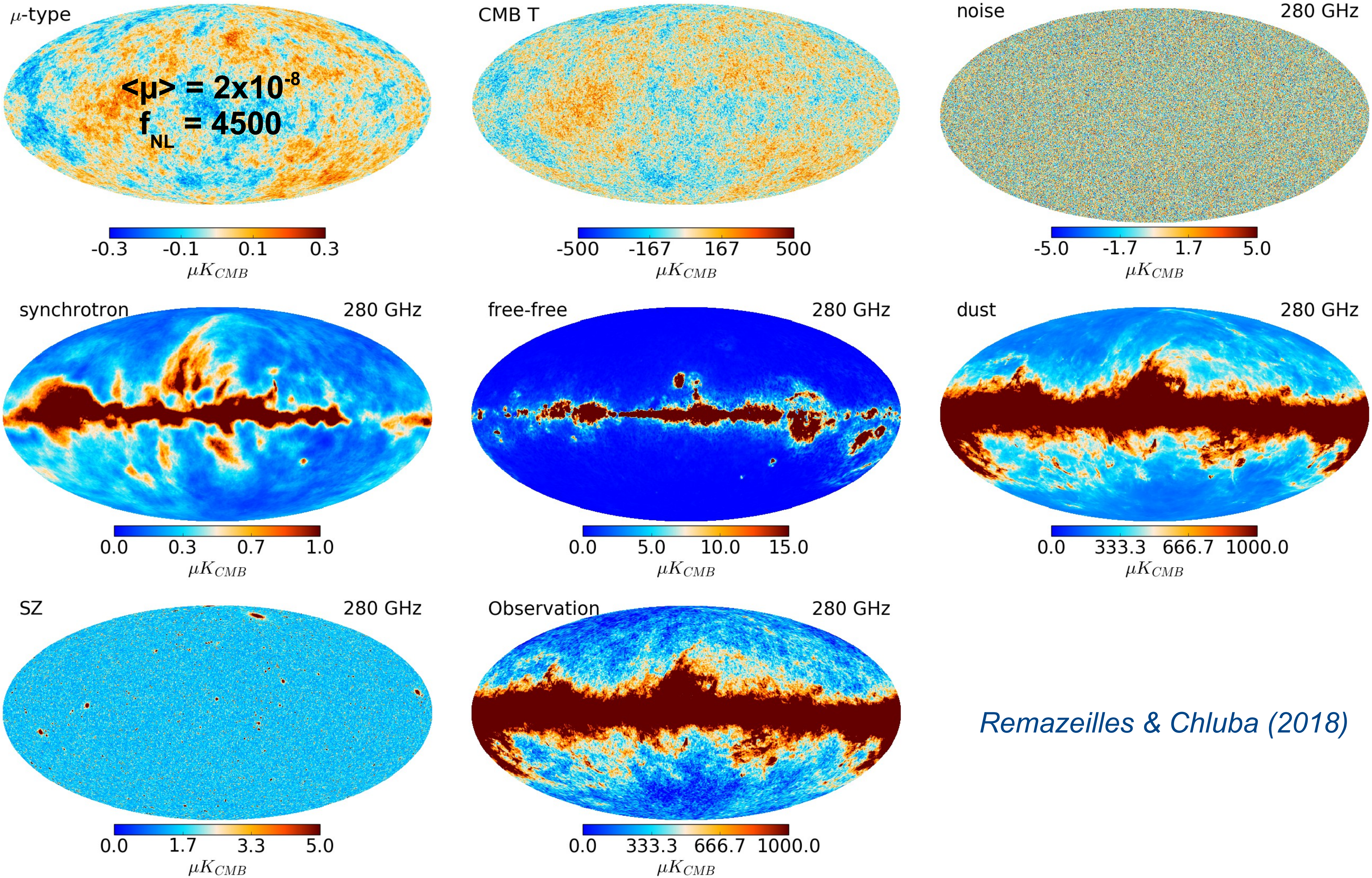

Remazeilles & Chluba (2018)

Constrained ILC μ-map reconstruction (LiteBIRD)

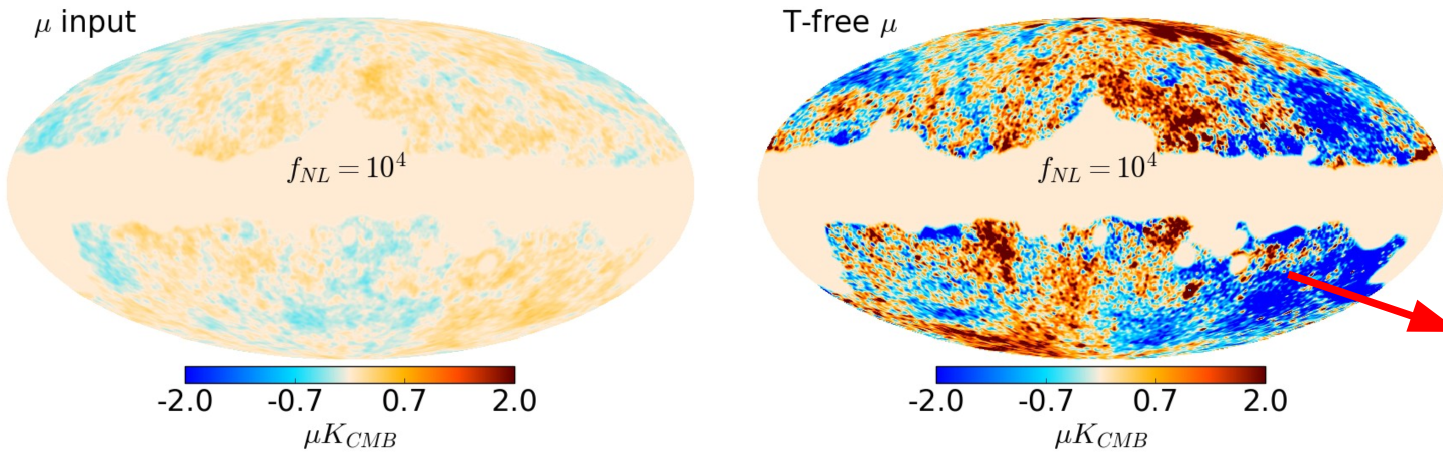

significant foreground contamination

Remazeilles & Chluba (2018)

Constrained ILC μ-map reconstruction (LiteBIRD)

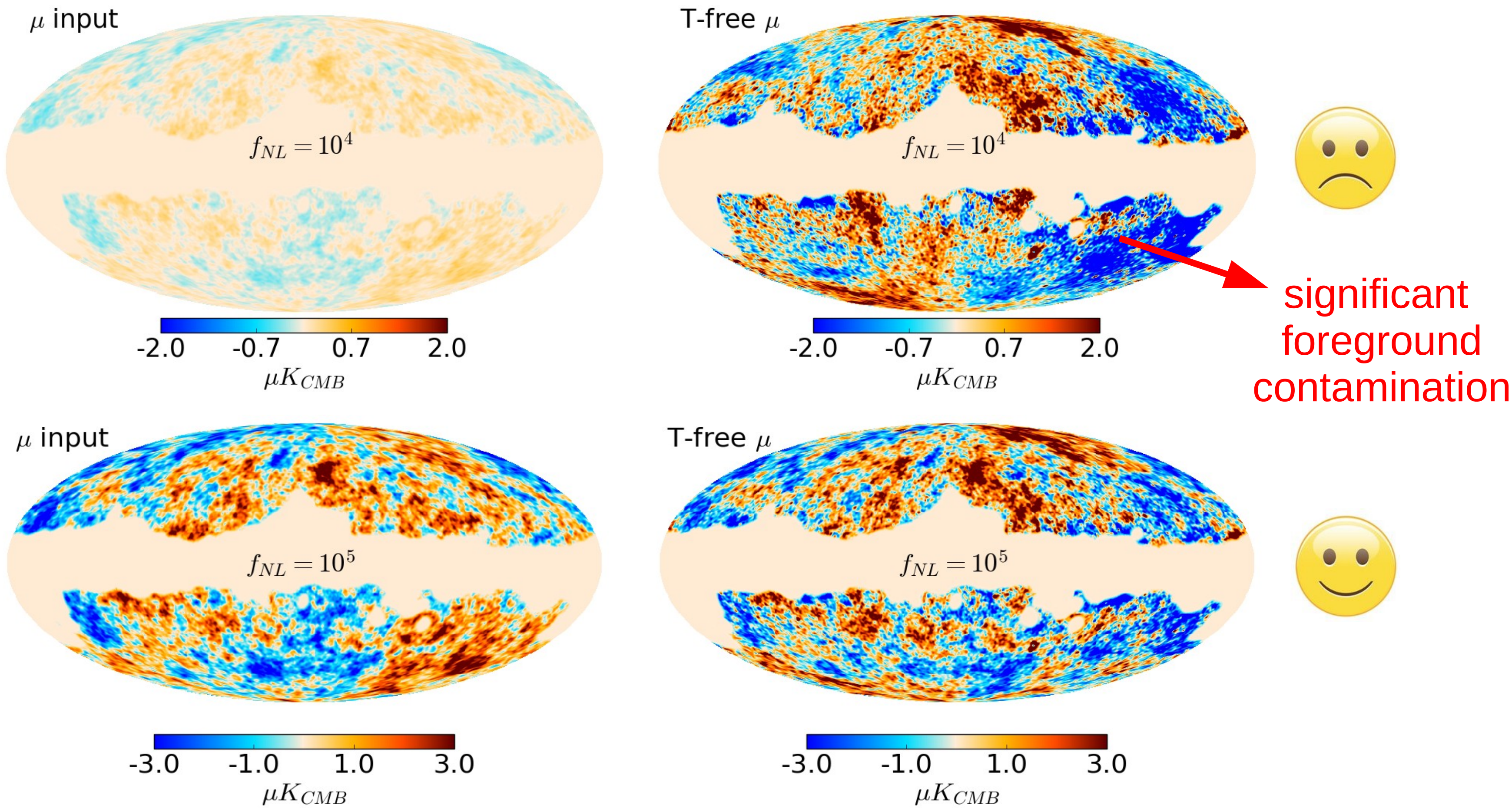

Remazeilles & Chluba (2018)

Constrained ILC μ-map reconstruction (LiteBIRD)

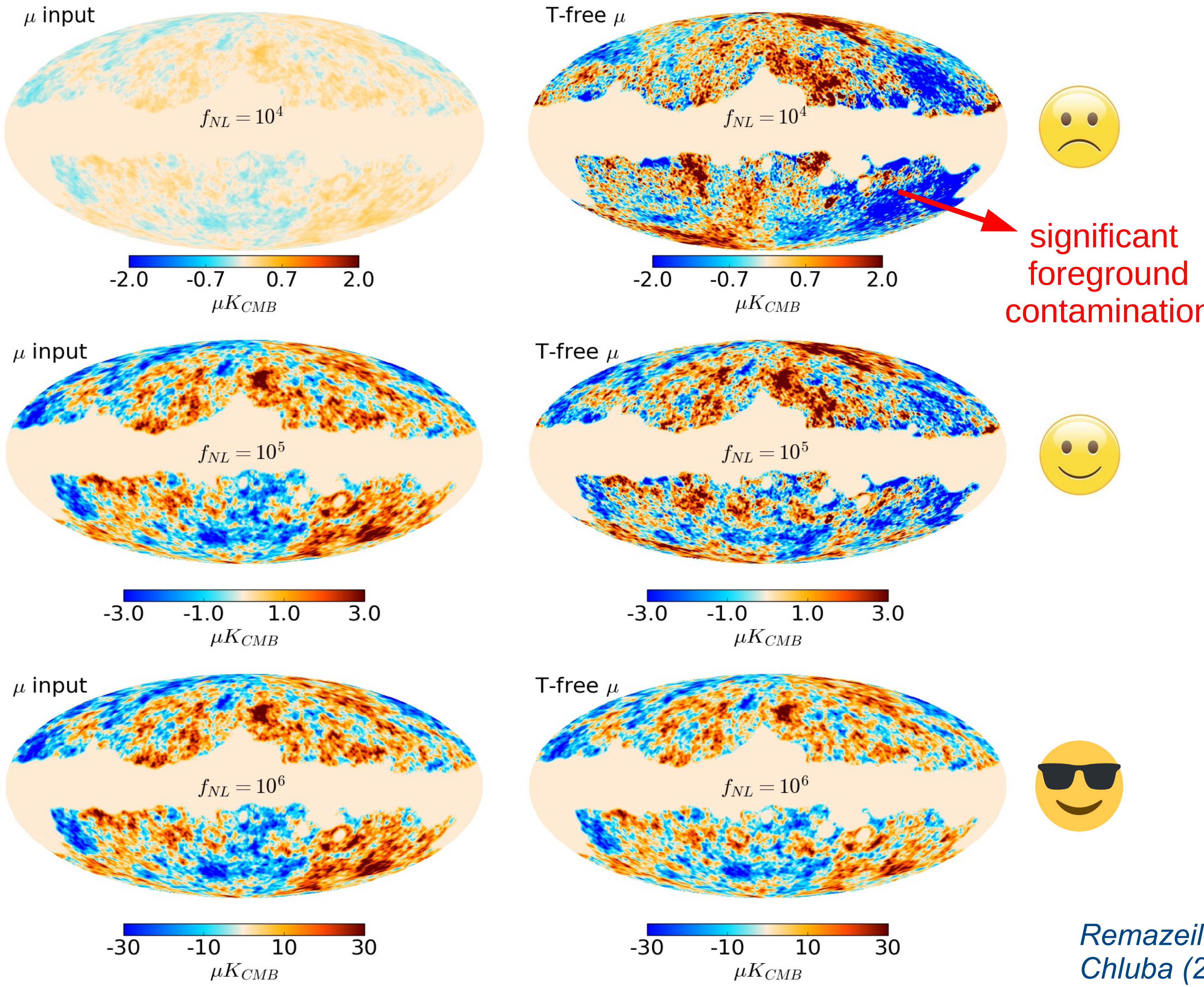

Remazeilles & Chluba (2018)

Constrained ILC μ-map reconstruction (LiteBIRD)

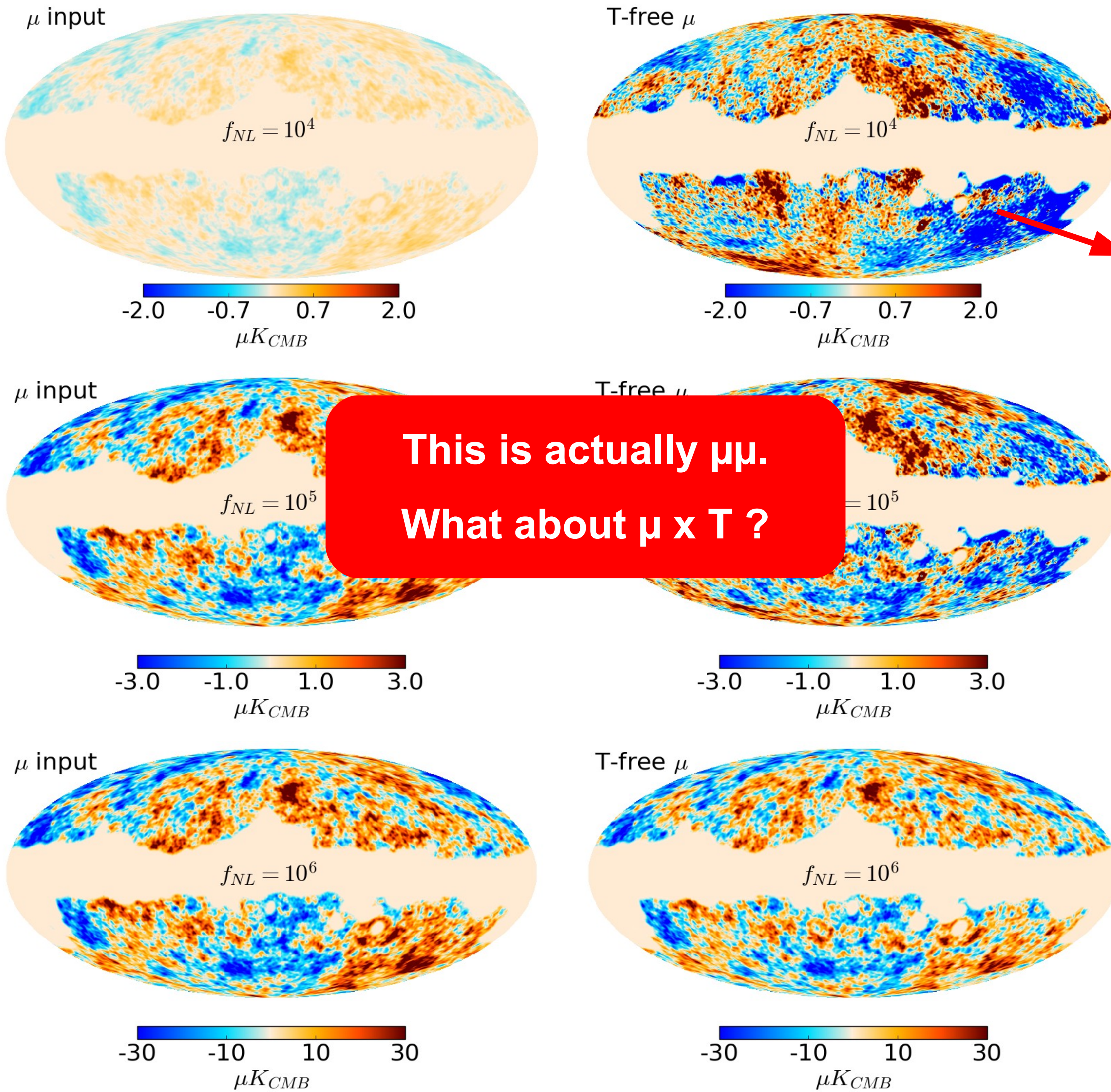

This is actually μμ.

What about μ x T ?

significant foreground contamination

Remazeilles & Chluba (2018)

$C_\ell^{\mu\times T}$ reconstruction: $f_{NL} = 4500$ (w/o foregrounds)

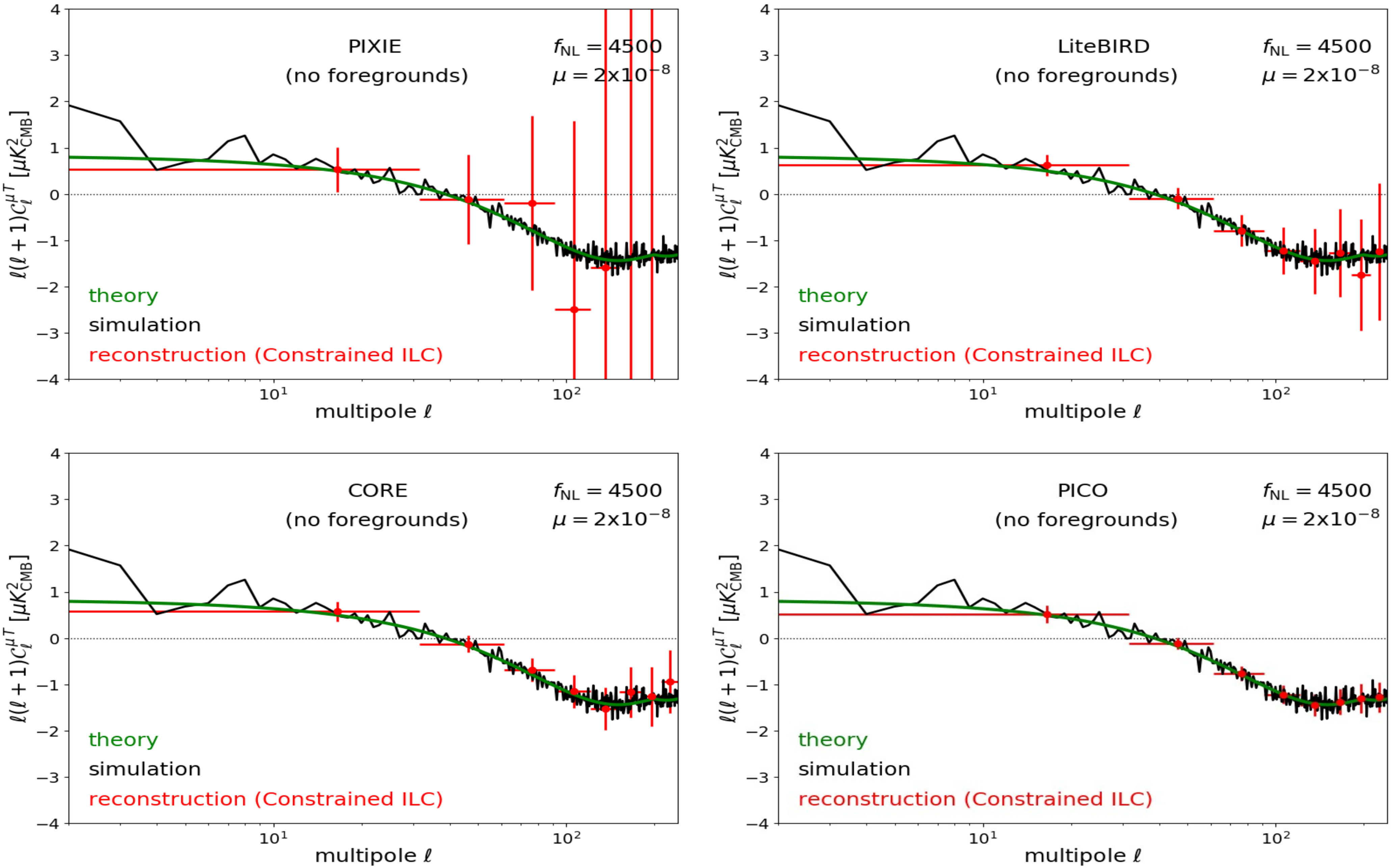

Remazeilles & Chluba (2018)

$C_\ell^{\mu\times T}$ reconstruction: $f_{NL} = 4500$ (with foregrounds)

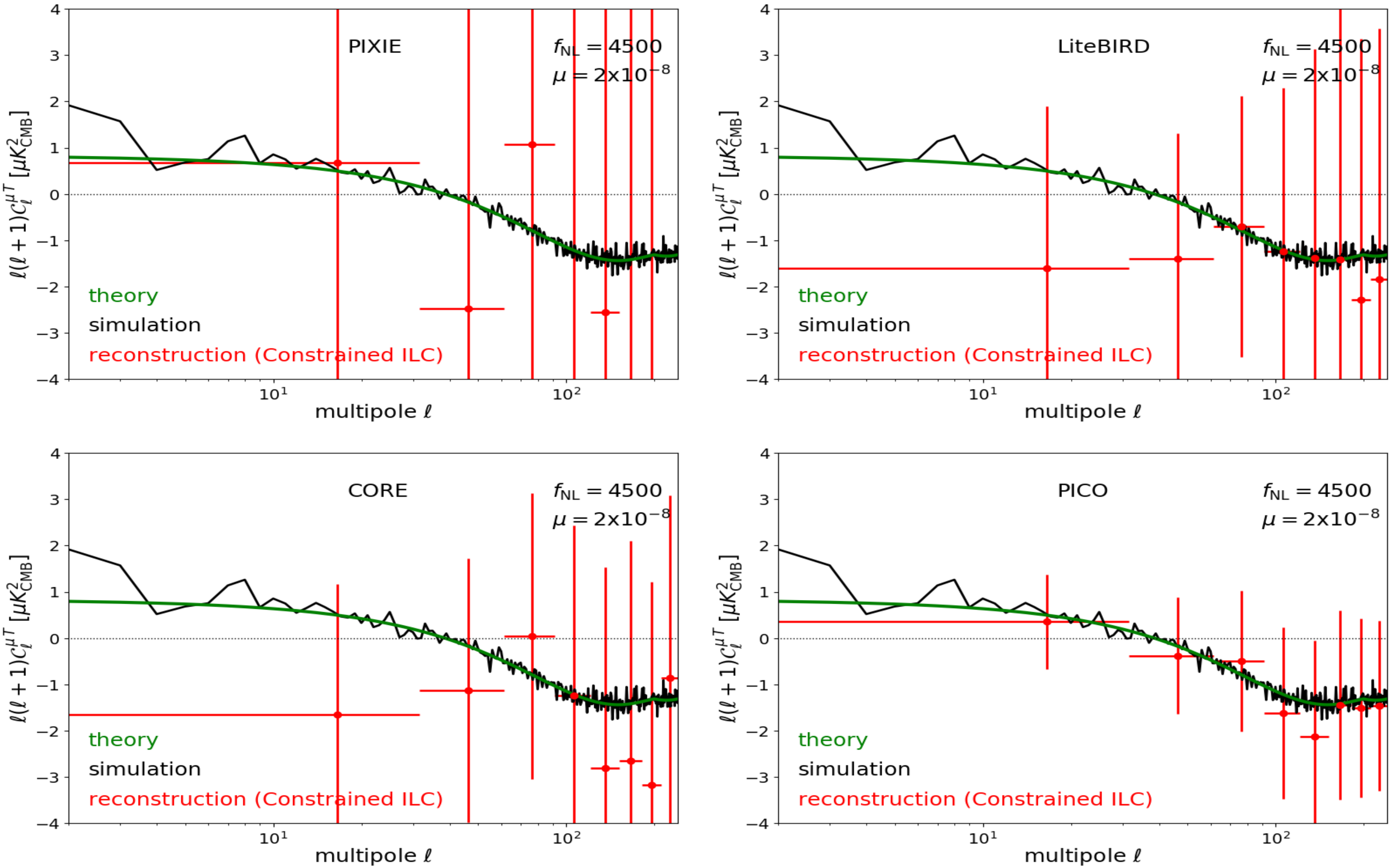

Remazeilles & Chluba (2018)

$C_\ell^{\mu\times T}$ reconstruction: $f_{NL} = 4500$ (with foregrounds)

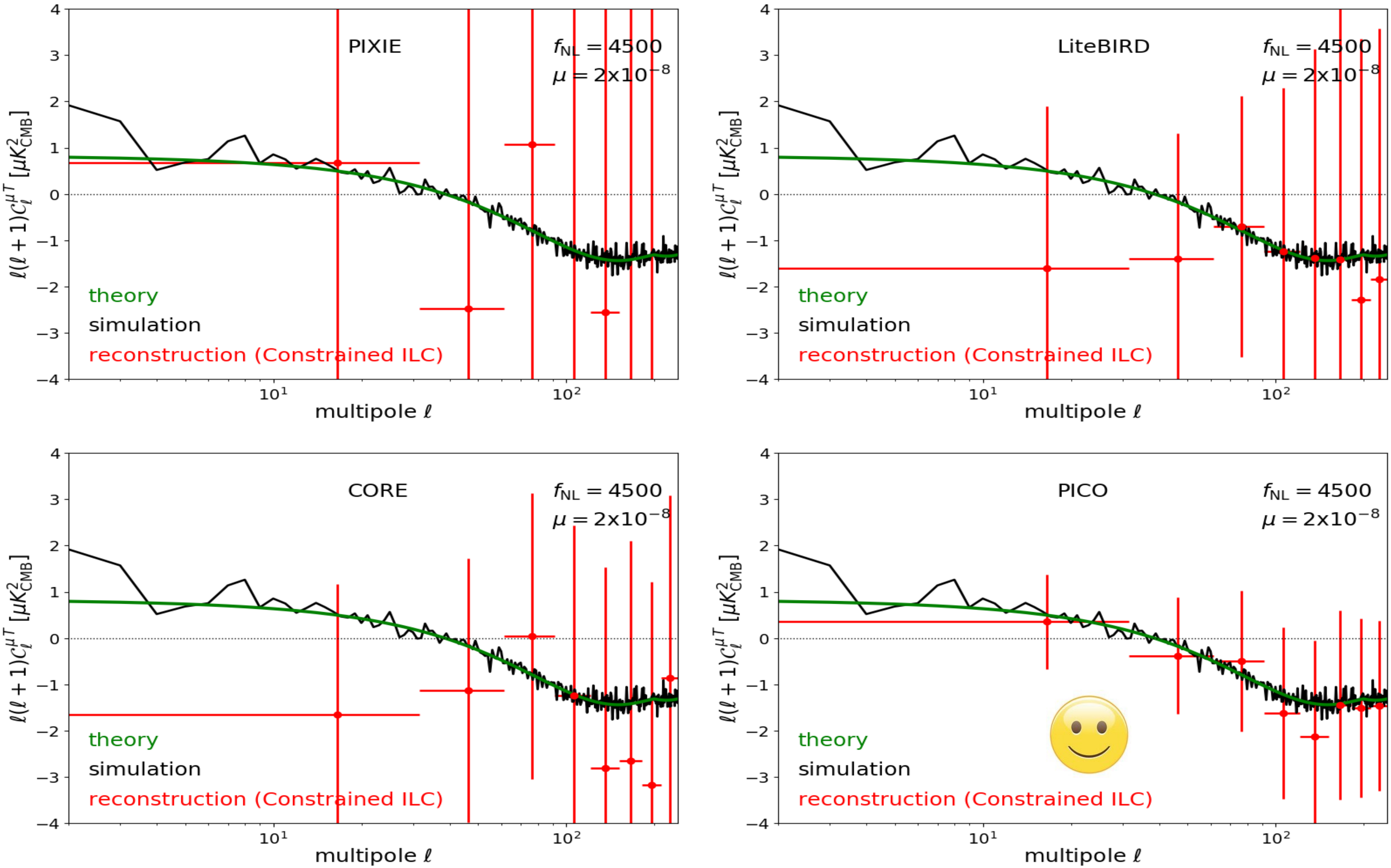

Remazeilles & Chluba (2018)

$C_\ell^{\mu \times T}$ reconstruction: $f_{NL} = 10^4$ (with foregrounds)

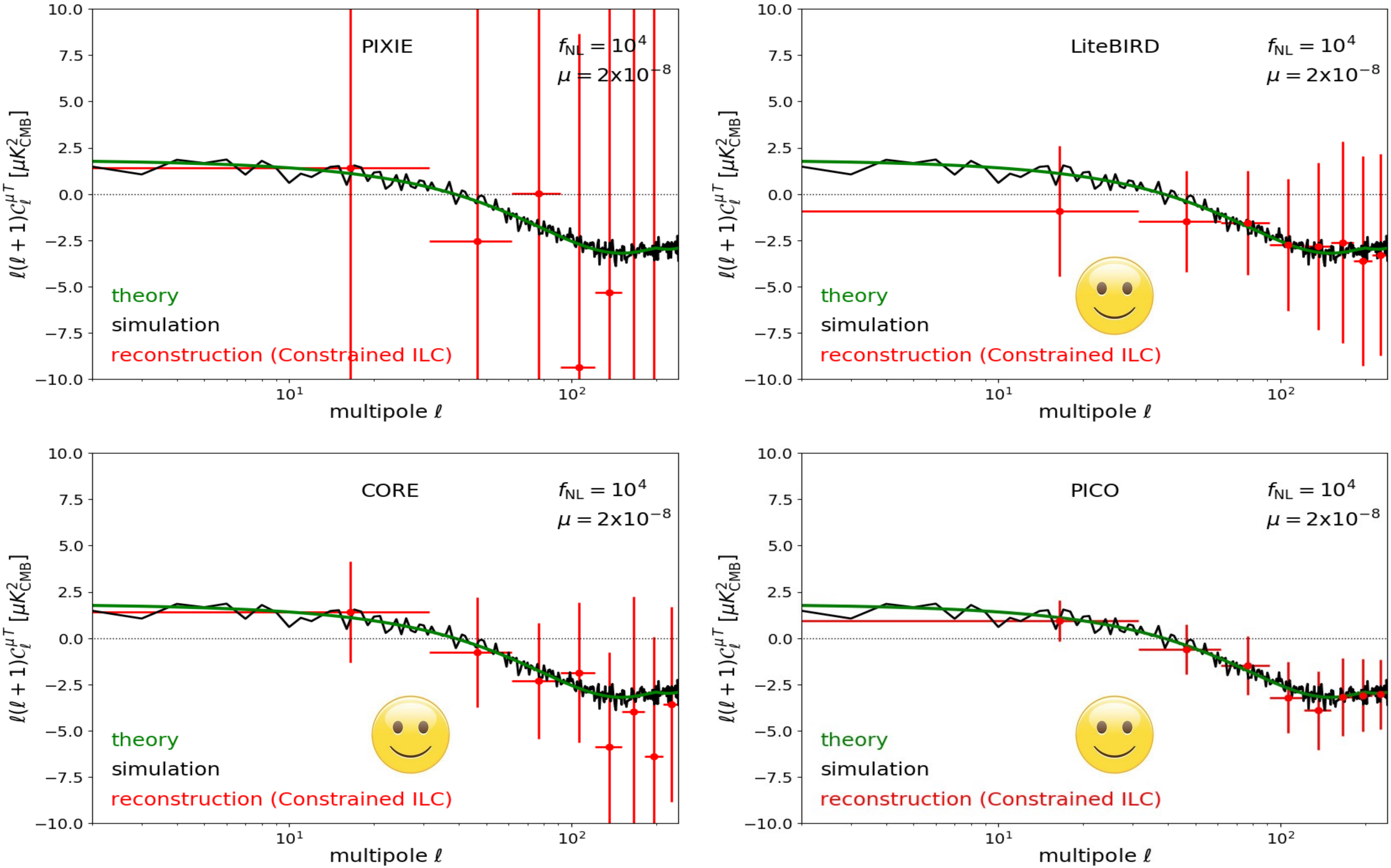

Remazeilles & Chluba (2018)

$C_\ell^{\mu\times T}$ reconstruction: $f_{NL} = 10^5$ (with foregrounds)

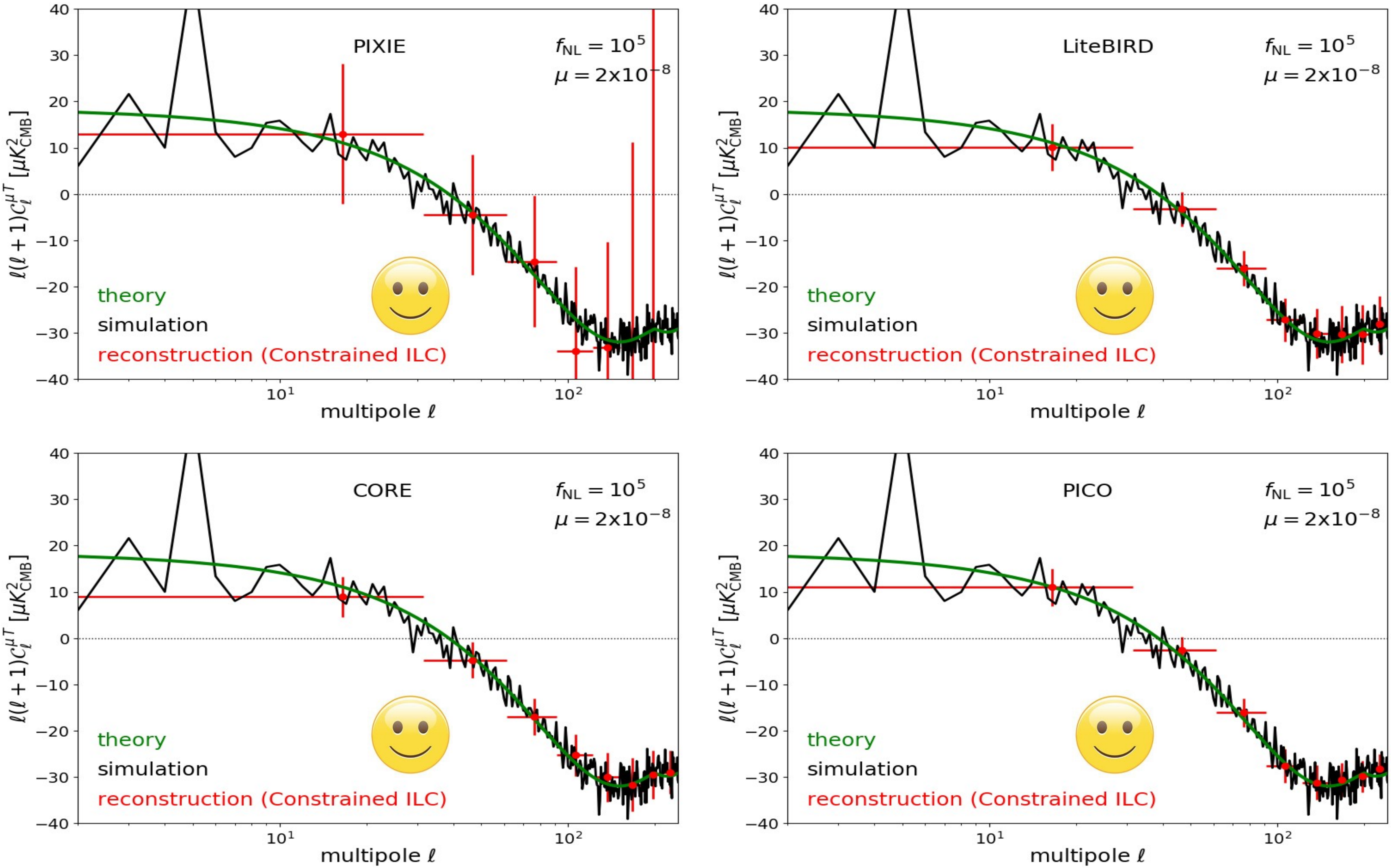

Remazeilles & Chluba (2018)

Standard ILC vs Constrained ILC

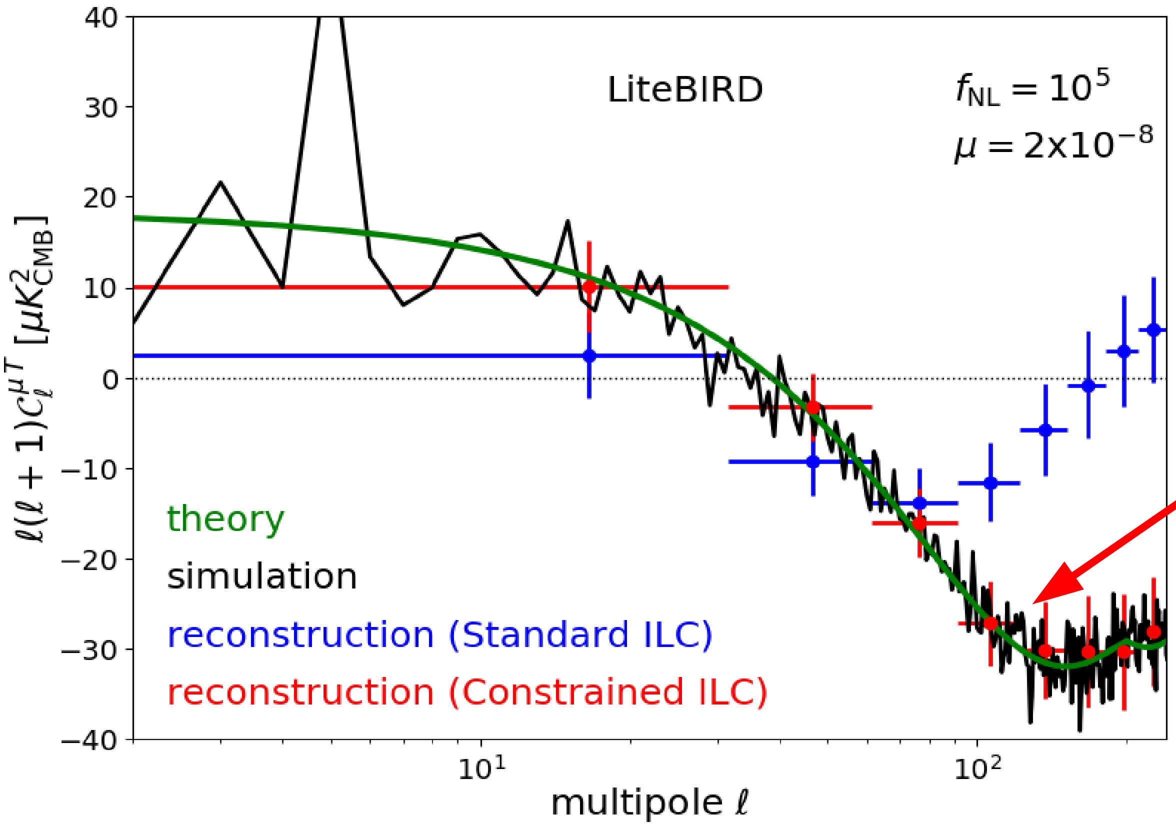

Standard ILC methods suffer from spurious TT correlations due to CMB residuals in the μ-map

The Constrained ILC fully recovers the correlated μ-T signal

In light of these considerations,
the constraints on μT from Planck data (Khatri & Sunyaev 2015) should be taken cautiously

Remazeilles & Chluba (2018)

Forecasts on primordial non-Gaussianity

Table 5. Detection forecasts on $f_{\rm NL}(k \simeq 740\,{\rm Mpc}^{-1})$ after component separation, based on multipoles $2 \leqslant \ell \leqslant 200$.

$f_{\rm NL}$ (fiducial)	10^5	10^4	4500	4500 w/o foregrounds
PIXIE	$(1.11 \pm 0.40) \times 10^5$	$(2.17 \pm 3.90) \times 10^4$	$(1.5 \pm 3.9) \times 10^4$	4778 ± 3868
	2.5σ	–	–	1.2σ
LiteBIRD	$(0.98 \pm 0.08) \times 10^5$	$(0.91 \pm 0.68) \times 10^4$	4272 ± 6788	4753 ± 930
	12.5σ	1.5σ	–	4.8σ
CORE	$(0.97 \pm 0.08) \times 10^5$	$(1.35 \pm 0.74) \times 10^4$	5692 ± 6397	4336 ± 653
	12.5σ	1.4σ	–	6.9σ
PICO	$(0.99 \pm 0.06) \times 10^5$	$(1.07 \pm 0.30) \times 10^4$	5094 ± 2929	4480 ± 371
	17.8σ	3.3σ	1.5σ	12.1σ

Remazeilles & Chluba (2018)

Forecasts on primordial non-Gaussianity

Table 5. Detection forecasts on $f_{\mathrm{NL}}(k \simeq 740\,\mathrm{Mpc}^{-1})$ after component separation, based on multipoles $2 \leqslant \ell \leqslant 200$.

f_{NL} (fiducial)	10^5	10^4	4500	4500 w/o foregrounds
PIXIE	$(1.11 \pm 0.40) \times 10^5$ 2.5σ	$(2.17 \pm 3.90) \times 10^4$ –	$(1.5 \pm 3.9) \times 10^4$ –	4778 ± 3868 1.2σ
LiteBIRD	$(0.98 \pm 0.08) \times 10^5$ 12.5σ	$(0.91 \pm 0.68) \times 10^4$ 1.5σ	4272 ± 6788 –	4753 ± 930 4.8σ
CORE	$(0.97 \pm 0.08) \times 10^5$ 12.5σ	$(1.35 \pm 0.74) \times 10^4$ 1.4σ	5692 ± 6397 –	4336 ± 653 6.9σ
PICO	$(0.99 \pm 0.06) \times 10^5$ 17.8σ	$(1.07 \pm 0.30) \times 10^4$ 3.3σ	5094 ± 2929 1.5σ	4480 ± 371 12.1σ

PICO is in the best position to detect the μ-T correlation signal at $f_{NL}(k=740\ \mathrm{Mpc}^{-1}) \lesssim 4500$ in the presence of foregrounds

Remazeilles & Chluba (2018)

Pause

Despite a very broad frequency coverage, PIXIE results on anisotropic μ are of poorer quality than those from PICO, CORE, LiteBIRD

Why?! → *because of lower sensitivity and lower spatial resolution*

- We find that increasing PIXIE resolution from 96' to 40', while keeping the baseline sensitivity, would improve $\sigma(f_{NL})$ by 50%

  → *high-resolution channels enable using more spatially correlated information to improve foreground cleaning*

- If the foreground complexity can be captured by, say, 10 degrees of freedom, then 15-20 frequency bands are enough to remove the foregrounds

  → *In this case, the most sensitive experiments will make a difference in the ILC trade-off of minimizing the balance between foreground and noise contamination*

- If the foreground complexity relies on more than 20 degrees of freedom, then the broad frequency range of PIXIE will make a difference with respect to imagers

Remazeilles & Chluba (2018)

μ-T reconstruction for $f_{NL} = 0$

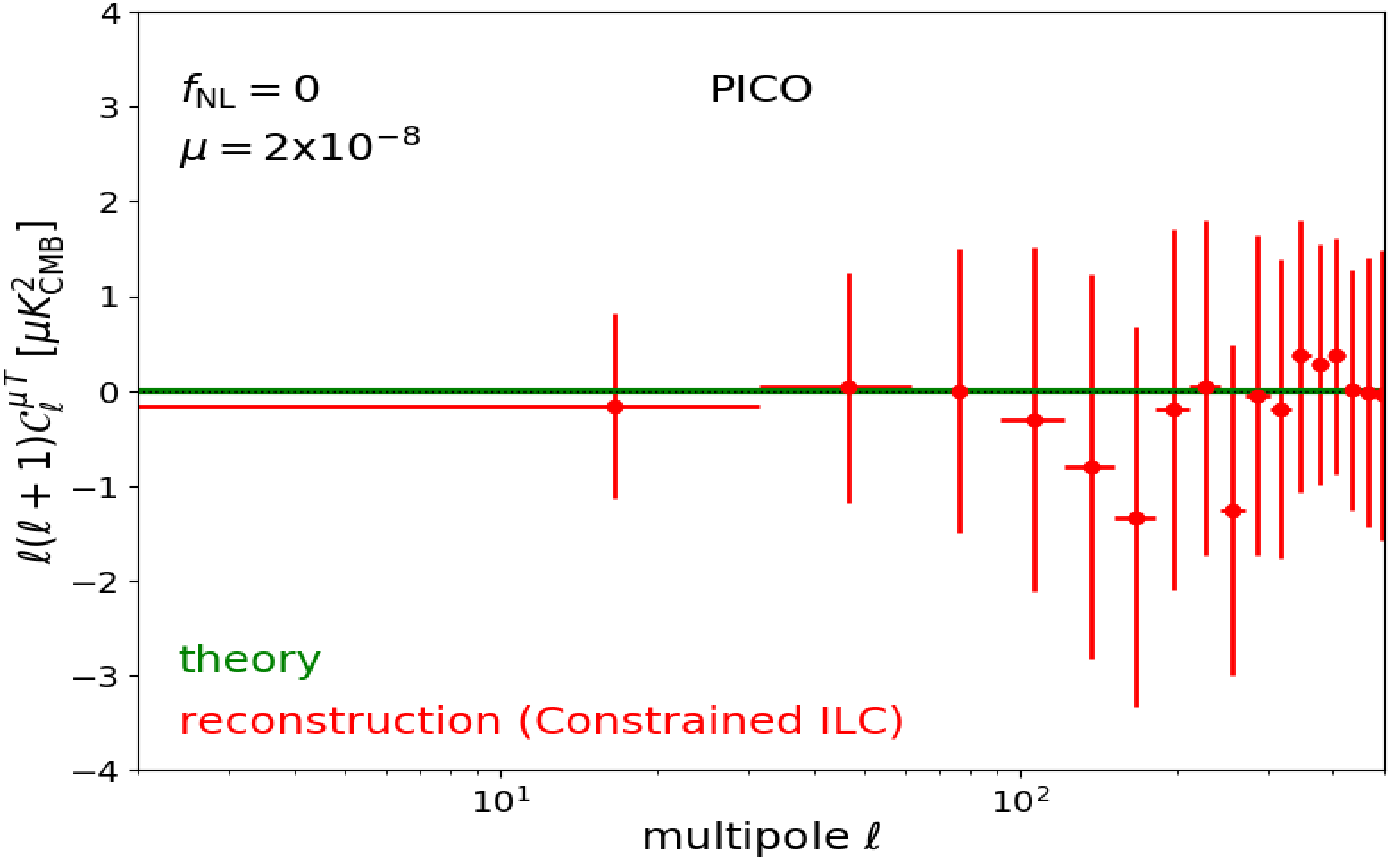

In the absence of μ-distortion anisotropies, the reconstruction by Constrained ILC is consistent with $f_{NL} = 0$

Remazeilles & Chluba (2018)

Minimum detection limit

Table 6. Detection limits for *PICO* on $f_{\rm NL}$ ($k \simeq 740\,{\rm Mpc}^{-1}$) after component separation, based on the multipole range $2 \leqslant \ell \leqslant 500$ using the model of Ravenni et al. (2017) to describe the $\mu - T$ cross-correlation. Foregrounds are included in all cases and the fiducial $f_{\rm NL}$ parameter was varied.

$f_{\rm NL}$ (fiducial)	−4500	0	4500
PICO	-2996 ± 2112 2σ	1325 ± 2114 –	5698 ± 2121 2σ

<u>Minimum detection limit by PICO in the presence of foregrounds</u>:

$$|f_{NL}| \leq 2114$$

Remazeilles & Chluba (2018)

More detectors or more frequencies?

“Super-LiteBIRD” with <u>100 x more detectors</u>

40 – 400 GHz, 0.2 μK.arcmin

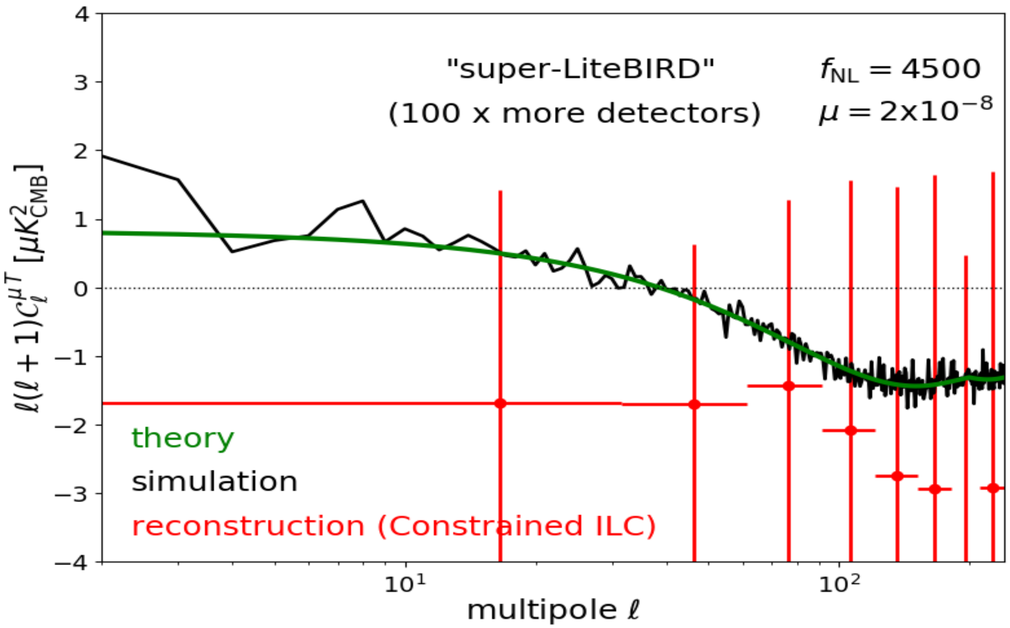

PICO baseline

20 – 800 GHz, 0.8 μK.arcmin

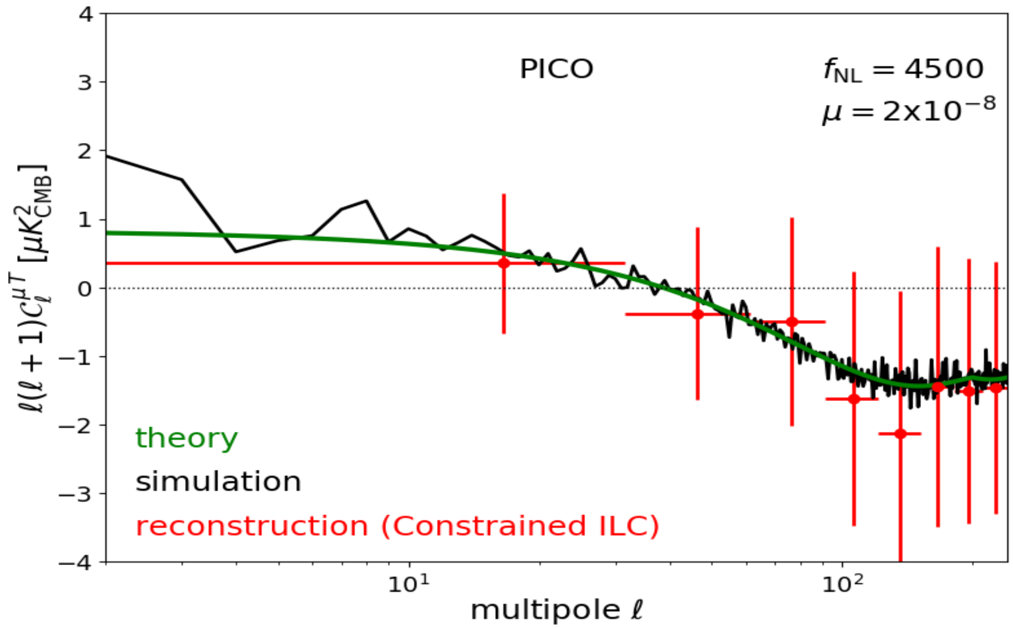

Extended frequency coverage at frequencies ν ≤ 40 GHz and ν ≥ 400 GHz provides more leverage than increased channel sensitivity

Remazeilles & Chluba (2018)

What part of the frequency range matters?

- Discarding PICO frequencies above $\nu > 400$ GHz degrades our component separation results by ~7%
- Discarding PICO frequencies below $\nu < 40$ GHz degrades our component separation results by ~30%

Low-frequencies $\nu \leq 40$ GHz have more constraining power for μ-distortion anisotropies than high-frequencies above $\nu \geq 400$ GHz

Remazeilles & Chluba (2018)

→ *consistent with the conclusions of Abitbol et al (2017) for monopole distortions*

Impact of inter-calibration errors

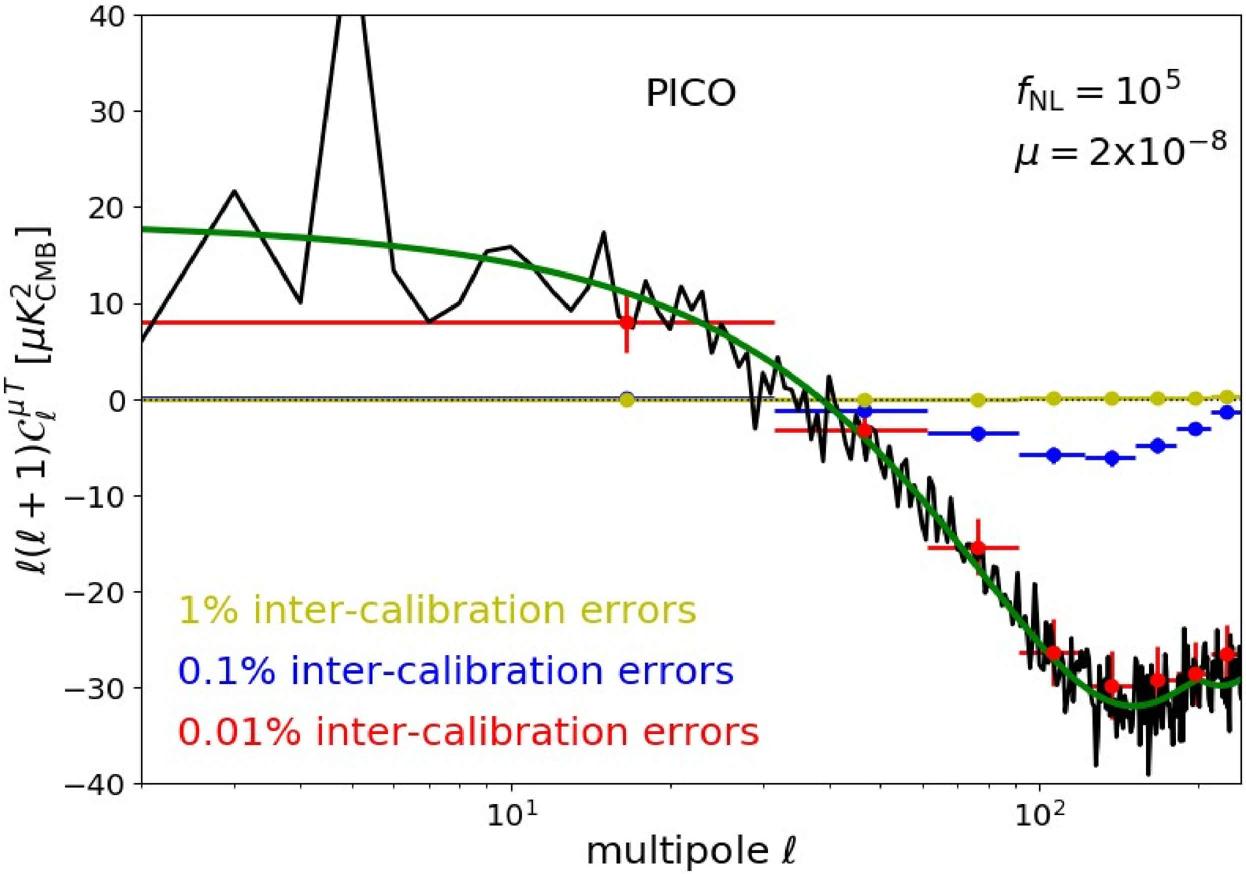

Dick, Remazeilles, Delabrouille, MNRAS (2010):
“ Calibration errors can screw up the ILC in the high signal-to-noise regimes, through partial cancellation of the variance of the CMB temperature map ”

The allowed inter-channel calibration uncertainty for PICO is 0.01 %

(The promise of CORE is to achieve such calibration accuracy)

Remazeilles & Chluba (2018)

Averaging effects

dust spectral indices in the sky

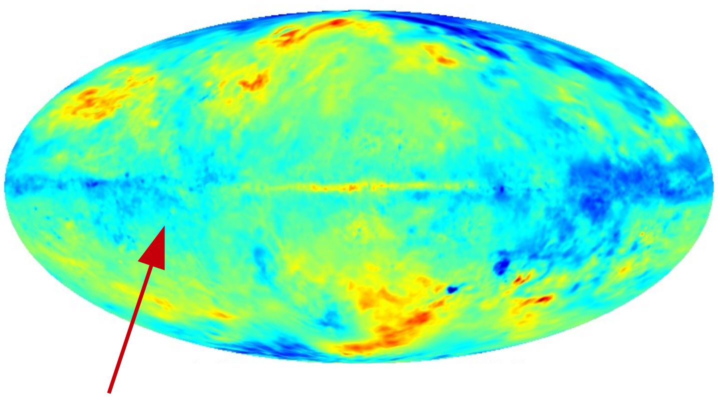

one value β_{dust} per line-of-sight

mapping / pixelization

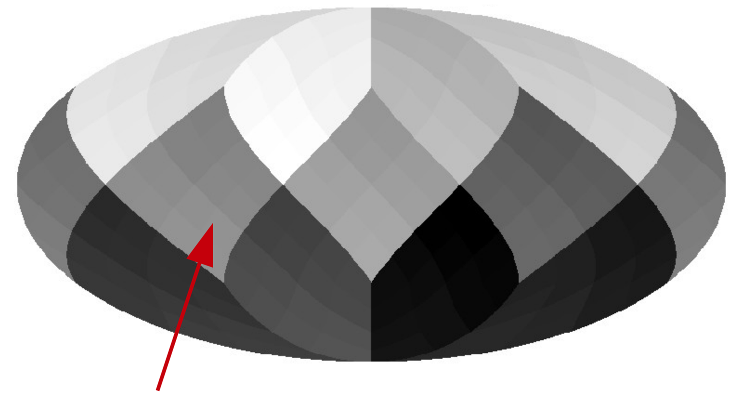

many β_{dust} values per pixel

$\rightarrow$ effective SED: $\sum_i \nu^{\beta i} \neq \nu^{\beta}$

- Because of averaging different line-of-sight SEDs within a pixel/beam, the actual SED of foregrounds *in the maps* will differ from the physical SED *in the sky* – *Chluba et al 2017*
- Spurious SED curvatures created by pixel averaging effects, if ignored in the parametric fit, have been shown to bias primordial B-modes at the level of $\Delta r \sim 10^{-3}$
  – *Remazeilles et al 2017, for the CORE collaboration*
- The “Constrained ILC” is blind (no parametrization / assumption on foregrounds), so fairly insensitive to averaging effects

Remazeilles & Chluba (2018)

Conclusions

Remazeilles & Chluba (2018)

- We have computed the first forecasts on the detection of the **μ-T correlation signal and f_{NL}(k≈740 Mpc^{-1}) in the presence of foregrounds with future CMB satellites**

- We have proposed a tricky component separation approach **(Constrained ILC)** to null the CMB contamination in μ, which otherwise biases the μ-T correlation signal

- Among the CMB satellite concepts, **PICO** is in the best position to control foregrounds and detect anisotropic μ-type distortions with **f_{NL}(740 Mpc^{-1}) ≲ 2100**

- Optimization: more detectors or more frequencies?

  Extended frequency coverage at frequencies ν ≤ 40 GHz and ν ≥ 400 GHz provides more leverage than increased channel sensitivity

  Low-frequencies ν ≤ 40 GHz have more constraining power on anisotropic μ-distortions than high-frequencies ν ≥ 400 GHz

- Absolute calibration / FTS like PIXIE still needed for μ-distortion anisotropies to break the f_{NL}*<μ> degeneracy

Thank you for your attention!